

RESEARCH

Modeling Human Mobility considering Spatial, Temporal and Social Dimensions

Giuliano Cornacchia¹, Giulio Rossetti² and Luca Pappalardo^{2*}

*Correspondence:

luca.pappalardo@isti.cnr.it

²ISTI-CNR, Pisa, Italy

Full list of author information is available at the end of the article

Abstract

Modelling human mobility is crucial in several areas, from urban planning to epidemic modelling, traffic forecasting, and what-if analysis. On the one hand, existing models focus mainly on reproducing the spatial and temporal dimensions of human mobility, while the social aspect, though it influences human movements significantly, is often neglected. On other hand, those models that capture some social aspects of human mobility have trivial and unrealistic spatial and temporal mechanisms. In this paper, we propose STS-EPR, a modelling framework that embeds mechanisms to capture the spatial, temporal and social aspects together. Our experiments show that STS-EPR outperforms existing spatial-temporal or social models on a set of standard mobility metrics, and that it can be used with limited amount of information without any significant loss of realism. STS-EPR, which is open-source and tested on open data, is a step towards the design of a mechanistic models that can capture all the aspects of human mobility in a comprehensive way.

Keywords: human mobility; generative models; synthetic trajectories; social network; data science; mechanistic models

1 Introduction

Modeling the mechanisms that govern human mobility is of fundamental importance in different disciplines, such as computational epidemiology, traffic forecasting, urban planning, and what-if analysis [1, 2, 3, 4, 5, 6]. First of all, mobility data sets contain sensitive information about the individuals whose movements are described [7, 8, 9], making them expensive and difficult to obtain from providers, and rarely available publicly for scientific research. Individual mobility models, often referred to as generative algorithms of human mobility [10, 5, 11], can reproduce synthetic trajectories that are realistic in reproducing fundamental patterns of individual human mobility. A significant advantage of using generative models concerns the cost and the time spent in the data collection, which is negligible with respect to the acquisition of a real dataset. Moreover, using generative algorithms allows the simulation of the mobility for a set of agents in an unseen scenario, hence allowing complex what-if analysis.

Most individual models focus on capturing the spatial and temporal patterns of human mobility, such as the existence of a power-law distribution in jump lengths [12, 4, 13] and in the characteristic spatial spread of an individual [4], a strong tendency to return to locations they visited before [4] and a propensity to move following a circadian rhythm [2, 14]. However, the social dimension of human mobility is often neglected, despite the fact that about 10-30% of human movements can be

explained by social purposes [15]. The only model that takes into consideration the social dimension is GeoSim [16], which contemplates a mechanism related to the individual preference and social influence. Unfortunately, the temporal and spatial mechanisms of GeoSim are not realistic, making the model incomplete and hardly usable in practice.

In this paper, we propose STS-EPR, which combines the most realistic spatial, temporal and social mechanisms into one modelling framework. Namely, STS-EPR includes a mechanism that takes into account the spatial distance between locations as well as the relevance of a location [3, 17]. Second, STS-EPR includes a temporal mechanism based on a diary generator, a data-driven algorithm able to capture the tendency of individuals to follow a circadian rhythm [2]. Finally, our model includes social mechanisms inspired by GeoSim in order to model the social dimensions of mobility, too [16]. Finally, we include novel mechanisms related to social popularity and constraints in the location an agent can reach in a given time. We provide the code to reproduce our model and conduct experiments on an open data sets, hence making our work fully replicable and reproducible.

Our experiments on data describing the checkins of 1000 users in New York City show that the generated trajectories are realistic with respect to the social, temporal and mobility aspects, outperforming existing models on a set of standard mobility metrics. We further validate the modeling ability of STS-EPR, simulating the mobility of individuals moving in London, including in the model different levels of knowledge concerning their mobility behaviors, demonstrating that our model can be applied on different regions and with limited amount of information about that region without any significant loss of realism.

Our model is a further step towards the design of a three-dimensional generative models for human mobility, which combines the state-of-the-art spatial, temporal and social mechanisms with action-correction mechanisms specifying with borderline cases during the simulation.

2 Related Work

2.1 Human mobility patterns

The study of human mobility focuses on discovering and modeling the mechanisms that rule the movements of individuals and groups of individuals. In the last decade, researchers from several disciplines showed that that human mobility, far from being random, follows well-defined statistical laws [10, 5].

The seminal work by Brockmann et al. [12] analyzes nation-wide trajectories of dollar bills and finds that the distribution of the distance between two consecutive positions of a banknote follows a power-law. Subsequent studies confirm this finding on nation-wide trajectories of mobile-phone users [4] and region-wide trajectories of private vehicles [13, 17]. González et al. [4] find that, on nation-wide mobile phone data, the empirical distribution of the radius of gyration, the characteristic distance traveled by an individual, can be approximated with a truncated power-law; a statistical law confirmed on region-wide trajectories of private vehicles [13, 17].

Song et al. [3] find that the distribution of time between two displacements of an individual (waiting time), can be described by a truncated power-law and that the potential predictability of an individual's mobility is high [18]. Other laws regard

the existence of the returners and explorers dichotomy [17] and the conservation of the number of locations visited by an individual in a period of time [19].

Another strand of research demonstrates a strong relationship between human mobility and social ties [16, 20, 15, 21, 22]. First of all, friends have a higher probability of living or working together or having the same hobbies, increasing their mobility similarity compared with strangers [21]. Moreover, individuals are more likely to visit a location right after a friend has visited the same location, and the probability drops off following a power-law function [15]. Cho et al. [15] show that the probability for an individual to visit a friend remains constant as a function of the distance; Wang et al. [20] find that individuals with a similar visitation pattern are more likely to establish a social link.

2.2 Generative models

Building upon the above findings, many models have been proposed which try to reproduce the statistical laws of human mobility. For this paper's sake, we are interested in *mechanistic* generative models of human mobility [10].

The seminal paper by Song et al. [18] proposes the exploration and preferential return (EPR) model. EPR relies on two mechanisms: exploration and preferential return. The exploration mechanism is a random walk process with truncated power-law jump size distribution. The preferential return mechanism reproduces the propensity of humans to return to locations they visited before. If an agent returns to a previously visited location, it selects the location to visit with probability proportional to the number of times the agent visited that location. An agent in the model selects to explore a new location with probability P_{exp} , which decreases as the agent visits more and more locations. With complementary probability $P_{ret} = 1 - P_{exp}$, the agent returns to a previously visited location.

Several studies subsequently improved the EPR model by adding increasingly sophisticated mechanisms to reproduce statistical laws more realistically. In the d-EPR model [23], an agent visits a new location depending on both its distance from the current position and collective relevance. In the recency-EPR model [24], the preferential return phase includes information about the recency of location visits. In the memory-EPR model [19], during the exploration mechanism, the agent selects a location with probability proportional to the number of times it visited that location in the previous M days. EPR and its extension focus on the spatial aspect of human mobility, neglecting to reproduce realistic temporal patterns. For example, the displacements of individuals are not uniformly distributed during the day but follow the circadian rhythm, a property that is not captured by EPR-like models. Two refined models, namely TimeGeo [25] and DITRAS [2], overcome this problem by including a more sophisticated temporal mechanism.

TimeGeo [25] is a mechanistic modeling framework to generate individual mobility trajectories with realistic spatio-temporal properties. TimeGeo models the temporal dimension using a time-inhomogeneous Markov chain that captures the circadian propensity to travel and the likelihood of arranging short and consecutive activities [25]. It integrates the temporal mechanism with a rank-based version of the EPR model (r -EPR), which assigns a rank to each unvisited location during the selection of a new location to visit, depending on its distance from the trip origin [25].

DITRAS (DIary-based TRAJectory Simulator) [2] generates the trajectories using two probabilistic models: a diary generator and a trajectory generator. The diary generator is a Markov model trained on mobility trajectory data of real individuals, which captures the probability for individuals to follow or break their routine at specific times [2]; the diary generator builds a mobility diary with abstract locations for each agent in the simulation. The trajectory generator is an algorithm that, given a weighted spatial tessellation, translates the abstract locations in physical locations using the d-EPR model [3].

Despite the link between human mobility and social ties, the only mechanistic model that tries to reproduce the socio-mobility patterns is GeoSim [16]. GeoSim takes into account both the mobility and the social dimension, although incorporating a trivial temporal mechanism. GeoSim introduces two mechanisms in addition to the explore and preferential return ones: individual preference and social influence. The agent has to decide if its next displacements are influenced or not by its social contact, respectively, with probability α and $1 - \alpha$.

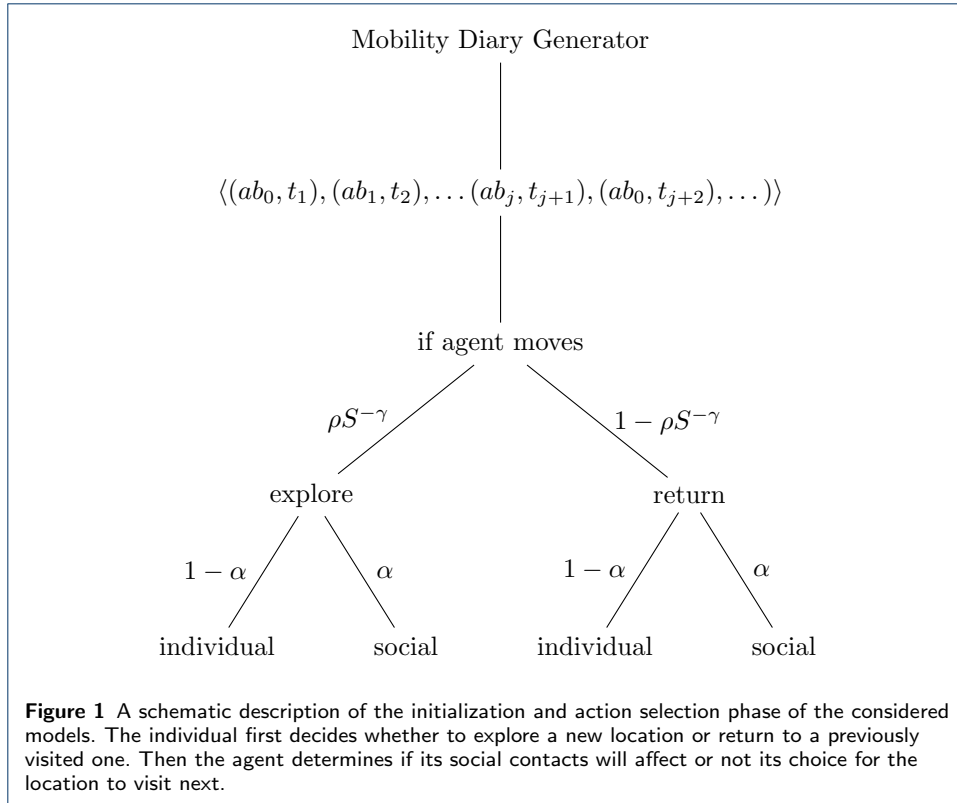
Position of our work. An overview of the literature cannot avoid noticing the lack of generative models able to reproduce the spatial, temporal, and social dimensions at the same time. On the one hand, GeoSim can capture important patterns describing the link between mobility and sociality, but cannot reproduce realistic spatio-temporal patterns. On the other hand, TimeGeo and DITRAS well reproduce spatial and temporal patterns but neglect the social dimension. In this paper, we build the STS-EPR model combining the mechanisms of existing mechanistic models to reproduce the three dimensions of human mobility.

3 Modeling Spatial, Temporal and Social patterns

We define a mobility trajectory as a sequence $T = \langle (r_1, t_1), \dots, (r_n, t_n) \rangle$ where t_i is a timestamp such that $\forall i \in [1, n) t_i < t_{i+1}$ and r_i is defined as (x_i, y_i) where the components are coordinates on a bi-dimensional space. In particular, we assume that individuals move on a weighted spatial tessellation L , representing the tiling of a bi-dimensional space, resulting in a non-overlapped set of locations. Every location has a weight corresponding to its relevance at a global level [2], and it has a representative point; generally, the centroid of the tile expressed as a pair of coordinates. $L = \langle (r_1, w_1), \dots, (r_n, w_n) \rangle$ where w_j is the weight of the tile j and r_j is the representative point of the tile j . We represent the visitation pattern of an individual a as a vector lv_a of $|L|$ elements, called location vector, where $|L|$ is the total number of locations. The j -th element of the location vector, $lv_a[j]$, contains the number of times a visited the location r_j . We also assume that the individual's network of contacts G influences their movements. $G = (V, E)$ is a graph in which V indicates the set of individuals and E the set of social ties between individuals. To capture the spatial, temporal, and social patterns simultaneously, we create STS-EPR.

3.1 STS-EPR

The spatial, temporal and social EPR model (STS-EPR) extends the EPR model by including the social dimension, taking in to account the fact that social purposes



can explain about 10-30% of the human movements [15]; and improving the temporal dimension, to accurately reproduce the distribution of the number of movements during the day. STS-EPR can simulate the mobility N agents, based on an undirected graph G modeling their sociality, a weighted spatial tessellation L modeling the geographic space, and a mobility diary generator MDG modeling daily mobility schedules.

STS-EPR consists of three phases: initialization, action selection, and location selection (Figure 1). After the initialization phase, the agents execute the action selection and location selection phases until a stopping criterion is satisfied (e.g., the number of hours to simulate is reached).

Initialization phase. In the initialization phase, the N agents are connected in an undirected graph G , describing the social links between agents. The weight assigned to each edge represents the mobility similarity between the linked agents. For each agent in the simulation, the model assigns a mobility diary produced by the mobility diary generator MDG, a Markov model trained on mobility trajectory data of real individuals, which captures the probability for individuals to follow or break their routine at specific times [2]. The diary generator builds a mobility diary with abstract locations for each agent in the simulation. A mobility diary MD for an agent a is defined as:

$$\text{MD}_a = \langle (ab_0, t_1), (ab_1, t_2), \dots, (ab_j, t_{j+1}), (ab_0, t_{j+2}), \dots \rangle \quad (1)$$

Where ab is an *abstract location*, ab_0 denotes the home location of the agent a , t_i is a timestamp and the visits between two home locations are called *run*. The physical locations visited by an agent during a *run* must be distinct from each other, but the physical location resulting from the mapping of ab_i can be different in different runs. The abstract location ab_0 is assigned randomly to a physical location $r_j \in L$. Each agent will move according to the entries in its mobility diary at the time specified; if the current abstract location is ab_0 , the agent visits the home location, otherwise converts the abstract location into a physical one through the action and location selection steps.

Action selection phase. When an agent moves, it first decides whether to explore a new location or return to a previously visited one by selecting one of two competing mechanisms: exploration and preferential return. The exploration mechanism models the scaling law presented by Song et al. [3]: the tendency to explore new locations decreases over time. Preferential return reproduces individuals' significant propensity to return to locations they explored before [3, 2, 23]. An agent explores a new location with probability $P_{exp} = \rho S^{-\gamma}$, or returns to a previously visited location with a complementary probability $P_{ret} = 1 - \rho S^{-\gamma}$, where S is the number of unique locations visited by the individual and $\rho = 0.6$, $\gamma = 0.21$ are constants [3]. When the agent returns, it selects a location with a probability proportional to its visitation frequency.

At that point, independently of the spatial mechanism selected, the agent determines if the choice of the location to visit is affected or not by the other agents involved in the simulation, selecting between the individual and the social influence mechanisms. With a probability $\alpha = 0.2$ [16], the agent's social contacts influence their movement. With a complementary probability of $1 - \alpha$, the agent selects a location without the influence of the visitation pattern of the other agents.

Location selection phase After the agent selected one of the four possible combinations of the spatial and social mechanisms, it decides which location will be the destination of its next displacement. For an agent a , we define the sets containing the indices of the locations a can explore or return respectively, as follows:

$$exp_a = \{i \mid lv_a[i] = 0\} \quad (2)$$

$$ret_a = \{i \mid lv_a[i] > 0\} \quad (3)$$

The frequency of visits of an individual a relative to a location r_i is referred as $f_a(r_i) = \frac{lv_a[i]}{\sum_{j=1}^{|L|} lv_a[j]}$.

- **Spatial Exploration:** During the spatial exploration, an agent a chooses a new location to explore from the set exp_a . The power-law behavior of the probability density function of the jump length suggests that individuals are more likely to move at small rather than long distances. Individuals take into

account also the relevance of a location at a collective level together with the distance from their current location [2]. The method used for coupling both the distance and the relevance is the same used in the *d-EPR* model [23]: the use of a gravity law. Its accuracy justifies the gravity model's usage in estimating origin-destination matrices even at the country level [23]. An agent a currently at location r_j , during the Exploration-Individual action selects an unvisited location r_i , with $i \in \text{exp}_a$, with probability $p(r_i) \propto \frac{w_i w_j}{d_{ij}^2}$ where d_{ij} is the geographic distance between location r_i and r_j and w_i, w_j represent their relevance.

- **Social Exploration:** In the social exploration action, an agent a selects an agent c among its social contacts. The probability $p(c)$ for a social contact c to be selected is directly proportional to the mobility-similarity between them: $p(c) \propto \text{mob}_{sim}(a, c)$. After the contact c is chosen, the candidate location to explore is an unvisited location for the agent a that was visited by the agent c , more formally the location is selected from the set $A = \text{exp}_a \cap \text{ret}_c$; the probability $p(r_i)$ for a location r_i , with $i \in A$, to be selected is proportional to the visitation pattern of the agent c , namely $p(r_i) \propto f_c(r_i)$.
- **Individual Return:** In the individual return action, an agent a picks the return location from the set ret_a with a probability directly proportional to its visitation pattern. The probability for a location r_i with $i \in \text{ret}_a$ to be chosen is: $p(r_i) \propto f_a(r_i)$.
- **Social Return:** The contact c is selected as in the Exploration-Social action, while the set where the location is selected from is defined as $A = \text{ret}_a \cap \text{ret}_c$; the probability $p(r_i)$ for a location r_i to be selected is proportional to the visitation pattern of the agent c , namely $p(r_i) \propto f_c(r_i)$.

3.2 Additional features

To make STS-EPR more realistic, we include some additional features that model crucial aspects of human mobility in different and more complex scenarios.

Relevance-based Starting Locations. Given a weighted spatial tessellation L , during the initialization phase, the agents are assigned to a starting location r_i with a probability $p(r_i) \propto \frac{1}{|L|}$. With the introduction of the concept of relevance at a collective level for a location, we assign the agents at the starting location following the RSL principle (Relevance-based Starting Locations): the probability $p(r_i)$ for an agent of being assigned to a starting location r_i is $\propto w_i$, where w_i is the relevance of the location at a collective level.

Reachable locations. When an agent is allowed to move, it is associated with waiting time, specified in the mobility diary of the agent. The agent associated with a waiting time Δ_t cannot physically visit every location. Realistically, the agent should consider only the locations it can reach moving at a certain speed for the picked amount of time. We define speed_{agent} as the typical speed of an individual and I as the set of all the locations the agent can visit, the set R of the reachable locations for an agent starting from the location r_j is computed as follows:

$$R = \{i \in I \mid \text{dist}(r_j, r_i) \leq \text{dist}_{max}\} \quad (4)$$

where $dist_{max} = \Delta t \cdot speed_{agent}$

Social Choice by Degree. When an agent a performs a social action, selects a contact c with a probability $p(c) \propto mob_{sim}(a, c)$. The choice of social contact is personal for the agent; in fact, it is determined using only individual information, and no collective information is considered. During a social return, the selection process is the same as in the STS-EPR model. Instead, in social exploration, the contact is determined using its popularity at the collective level. The popularity pop of an individual u within a social graph G is defined as:

$$pop(u, G) = deg(u, G) \quad (5)$$

where the degree of a node n in the graph G is denoted as $deg(n, G)$. In the social exploration, an agent a selects a social contact c with probability $p(c) \propto pop(c, G)$. When an individual decides to explore a new location with a friend's influence, a popular friend will be more likely to influence its decision than an unpopular one, even if their mobility patterns are very different. For example, an event promoter (generally a popular node within a social graph) has a high probability of influencing one of its contacts, during the selection of the next location to explore, even though they can have different mobility behaviors. In contrast, when an individual decides to return at an already visited location with the influence of its social contacts, it is reasonable to think that the contact's choice is conducted using individual information. During the return action, individuals follow their routines. Consequently, they are more likely to select a contact with a similar mobility pattern.

Action-correction phase. The set of possible locations an agent can reach from the current one is limited and, in some extreme cases, can be empty. As an example, the agent cannot reach far away locations that would be reached at unrealistic speeds. It may also happen that all locations on the spatial tessellation have been visited at least once, and so there are no new locations to explore. To comply with these constraints, we include an action-correction phase, which is executed after the location selection phase, if the latter is too restrictive and does not allow movements in any location.

- **No new location to explore:** When an agent a performs the selection action phase (Figure 1) and decides to explore individually an unvisited location, it selects the location from the set exp_a (Equation 2). In case the agent visited all the locations on the spatial tessellation at least once, no choice can be made since $exp_a = \emptyset$. We deal with this case correcting the action (Figure 2) of the agent from Exploration-Individual to Return-Individual, preserving in this way the choice of performing the location selection without any influence of its social contacts.
- **No location in social choices:** If an agent a decides to move with the influence of a social contact c , and the set A computed for the relative action $A = ret_a \cap ret_c$ or $A = exp_a \cap ret_c$ is empty, we correct the action from the current to Return-Individual (Figure 2).

- **No reachable locations:** When an individual is allowed to move, it is associated with a waiting time Δt , and it can reach the locations in the set R (Eq. 3.2). The set R may be empty even if $I \neq \emptyset$, meaning there is no location the agent can visit within the radius $dist_{max}$ but the set of possible choices is not empty. If the agent was performing an exploration, a new $\Delta t_1 > \Delta t$ is selected to expand the area the agent can cover during its displacement. After picking the new waiting time the set R is computed, if $R = \emptyset$ then a new $\Delta t_2 > \Delta t_1$ is picked, (this procedure is repeated for a maximum of n_{max} time) and an Exploration-Individual action is performed with the new waiting time. If the agent was performing a Return-Social action or in the case the incrementing of the waiting time was performed n_{max} times, then the action is corrected with a Return-Individual; note that Return-Individual can not fail, since the agent can always return in its current location r_j from the moment that $dist(r_j, r_j) = 0$ (Figure 3).
- **Run in the Mobility Diary:** In the mobility diary the locations visited by an agent during a *run* (defined as the visits between two home return) must be distinct from each other. Given a run $d = \langle ab_1, ab_2, \dots, ab_n \rangle$ of length n , all the abstract locations $ab_i \in d$ must be assigned to distinct physical locations, the mapping between the abstract locations in d and the real locations in L must be injective. The injectivity of the mapping can not always be guaranteed: the location selection can fail due to the three cases presented above. With the use of the mobility diary, also the Individual-Return action can fail, since the agent can not even visit its current location. In the action correction phase (Figure 4), if a social choice cannot be completed, the next action executed is the action with the same mechanism performed without the influence of social contacts. In the case an individual action can not be performed, the complementary individual action is performed. If even the complementary individual action fails, the agent returns to the home location. When an agent returns to the home location due to action failure during the assignment of the abstract location $ab_j \in d$, the run d is splitted in $d1 = \langle ab_1, \dots, ab_j \rangle$, $d2 = \langle ab_{j+1}, \dots, ab_n \rangle$ and the agent start the mapping of the new run $d2$.

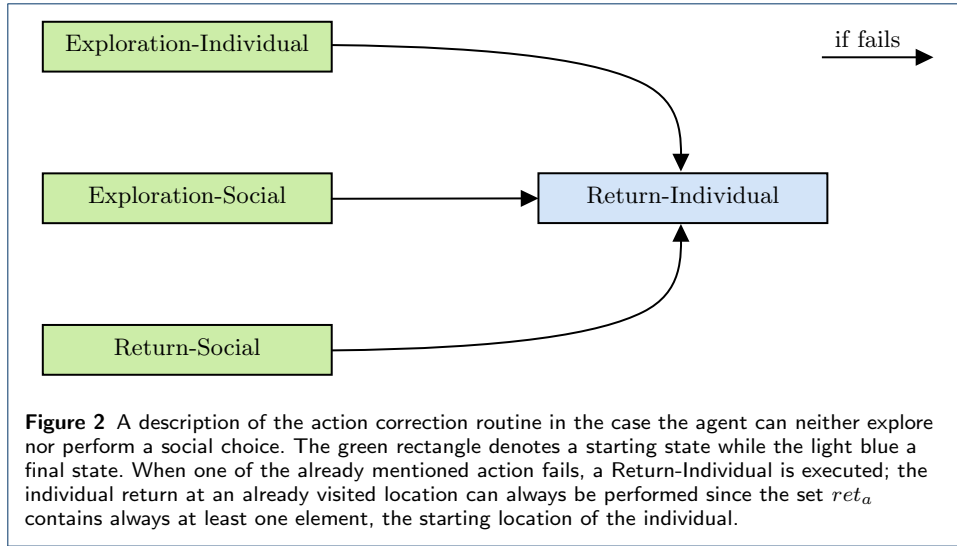
4 Results

In this chapter, we show the results of the experiments that simulate the mobility of 1,001 agents in the urban area of New York City for an observation period of three months. We compare the synthetic trajectories with the trajectories of the real individuals moving in the same city for the same number of months. We use a set of well-known mobility measures to assess the similarity between the two sets of trajectories.

4.1 Mobility Measures

We can classify the socio-mobility measures along the spatial, temporal, and social dimensions [14]. All the measures, except the social one, are computed through the *scikit-mobility*^[1] library [26].

^[1]<https://github.com/scikit-mobility>



Jump Length

A key factor in modeling human mobility is the distance an individual travels in an amount of time. Given a trajectory, the jump length Δr is the geographical distance between two consecutive locations visited by an individual u [4, 13]:

$$\Delta r = dist(r_i, r_{i+1}) \quad (6)$$

where r_i and r_{i+1} are two consecutive spatial points in the trajectory of u and $dist$ is the distance on the spherical earth between two points.

Radius of Gyration

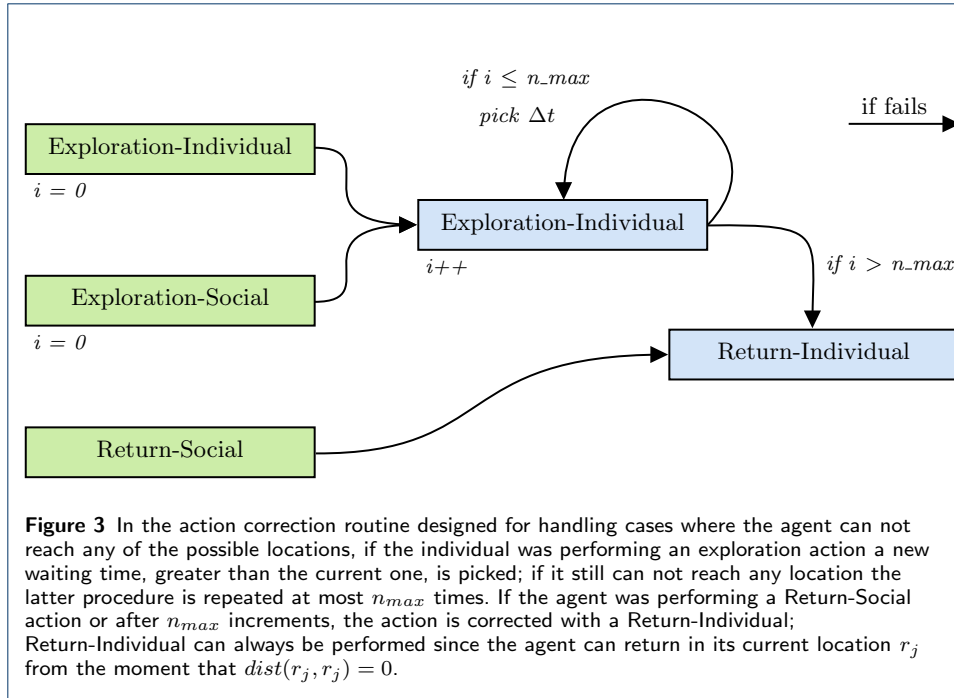
The radius of gyration $r_g(u)$ describes the typical distance traveled by an individual during the period of observation. It characterizes the spatial spread of the locations visited by the individual u from the locations' center of mass r_{cm} [4, 17].

$$r_g(u) = \sqrt{\frac{1}{N} \sum_{i=1}^N dist(r_i(u), r_{cm}(u))^2} \quad (7)$$

where N is the number of locations in the trajectory of the individual u and the center of mass $r_{cm} = \frac{1}{N} \sum_{i=1}^N r_i$.

Visits per Location

A useful measure to understand how individuals move in a physical space is the number of visits per location. This quantity describes the relevance of a location, namely the attractiveness at a collective level.



Location Frequency

Humans exhibit a strong tendency to return to locations they visited before [4]. The location frequency $f(r_i)$ measures the probability of visiting a location r_i :

$$f(r_i) = \frac{n(r_i)}{n_u} \quad (8)$$

where $n(r_i)$ is the number of visits to location r_i and n_u is the total number of points in the trajectory of the individual u .

One method to describe the importance of a location for an individual u is the concept of location's rank; a location r_i has rank k if it is the k -th most visited location by an individual u .

Waiting Time

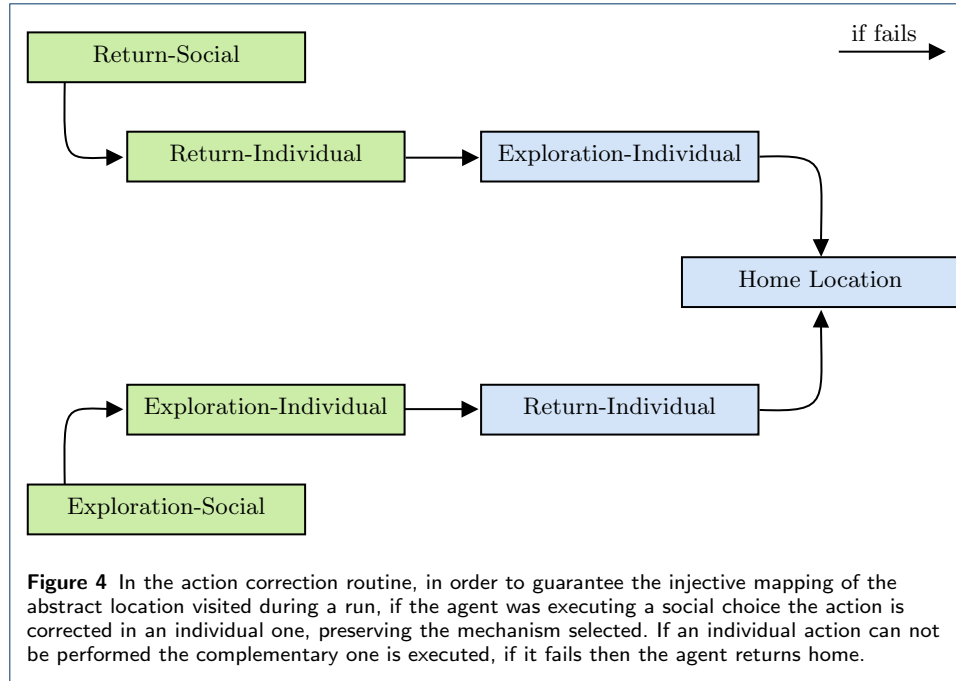
The waiting time Δ_t is defined as the elapsed time between two consecutive points in the mobility trajectory of an individual u , or equivalently as the time spent in a location:

$$\Delta_t = t_{i+1} - t_i \quad (9)$$

Uncorrelated Entropy

The uncorrelated entropy gives an estimation of the *predictability* of the movements of an individual u [18]:

$$E_{unc}(u) = - \sum_{i=1}^{N_u} p_u(i) \log_2(p_u(i)) \quad (10)$$



where N_u is the number of distinct locations visited by u and $p_u(i)$ is the historical probability that location i was visited by user u .

Activity per Hour

The movements of individuals are not distributed uniformly during the hours of the day. Humans' actions follow a circadian rhythm [2, 14]; people tend to be stationary during the night hours while they preferentially move at specific times of the day, for example, to reach the workplace or return home. To measure this distinctiveness of human mobility, we compute the number of movements made by the individuals at every hour of the day.

Mobility Similarity

Several studies demonstrate the correlation between human mobility and sociality [16, 20, 15, 21, 22]; the movements of friends are more similar than those of strangers, mainly because we are more likely to visit a location if a social contact explored that location before. Furthermore, individuals with a similar visitation pattern are more likely to establish a social link. We define the mobility similarity mob_{sim} between two individuals u_i, u_j as the cosine-similarity of their location vectors lv_i, lv_j .

$$mob_{sim}(u_i, u_j) = \frac{lv_i \cdot lv_j}{\|lv_i\| \|lv_j\|} \quad (11)$$

4.2 Statistical similarity

We quantify the statistical similarity between the distributions of the human mobility measures of the generated and the real trajectories using five metrics: [25, 2].

- **RMSE:** The Root Mean Square Error (RMSE) between a ground truth distribution p and a synthetic distribution q is defined as:

$$\text{RMSE}(p, q) = \sqrt{\frac{\sum_{i=1}^n (p_i - q_i)^2}{n}} \quad (12)$$

where $q_i \in q$, $p_i \in p$ and the number of observations in both the distributions is n .

- **Kullback–Leibler divergence:** The Kullback–Leibler divergence (KL) between a ground truth distribution p and a synthetic distribution q quantifies how much information is lost when q is used to approximate p .

$$\text{KL}(p \parallel q) = \sum_{i=1}^n p_i \log \left(\frac{p_i}{q_i} \right) \quad (13)$$

- **Hellinger distance:** The Hellinger distance (H) measure the distance between two distributions p and q .

$$\text{H}(p, q) = \frac{1}{\sqrt{2}} \sqrt{\sum_{i=1}^n (\sqrt{p_i} - \sqrt{q_i})^2} \quad (14)$$

- **Pearson’s correlation coefficient:** The Pearson’s correlation coefficient (r) is a measure of the linear relationship between two set of observations p and q .

$$r_{pq} = \frac{\sum_{i=1}^n (p_i - \bar{p})(q_i - \bar{q})}{\sqrt{\sum_{i=1}^n (p_i - \bar{p})^2} \sqrt{\sum_{i=1}^n (q_i - \bar{q})^2}} \quad (15)$$

where \bar{p} and \bar{q} are the mean values of p and q respectively.

- **Spearman’s Rank correlation coefficient:** The Spearman’s Rank correlation coefficient (ρ) measure the monotonic relationships (linear or non-linear) while Pearson’s correlation measure only linear relationships.

$$\rho_{pq} = 1 - 6 \frac{\sum_{i=1}^n (r_k(p_i) - r_k(q_i))^2}{n(n^2 - 1)} \quad (16)$$

where $r_k(p_i)$ is the *rank* of value p_i in the sorted list (p_1, \dots, p_n) , analogously $r_k(q_i)$.

4.3 Dataset

We compare the trajectories generated by STS-EPR with real trajectories obtained from an LBSN (Location-Based Social Network) data set collected by Yang et al. [22]. The data set contains a set of global-scale check-ins gathered from Foursquare over 22 months (from April 2012 to January 2014). A check-in describes a user’s real-time position with its social contacts. In Foursquare, the check-ins made by a user are not publicly available; despite this, many users share their check-ins on Twitter to make them public. The authors of the dataset collected the Foursquare

check-ins from Twitter by searching the Foursquare hashtag [22]. The dataset is associated with a lookup dataset for the locations, and with a snapshot of the social network obtained from Twitter, antecedent at the collection period.

The LBSN dataset D_{FS} [22], contains 90,048,627 check-ins made by 2,733,324 users all around the globe. The attributes of D_{FS} are an anonymized user identifier, an identifier of the location where the user made the check-in, the UTC (Coordinated Universal Time) when the check-in occurred, and the location's time-zone offset (Table 1). A lookup dataset D_{loc} associates the location's identifier with the respective coordinates and other information. LBSN datasets allow the reconstruction of the mobility of an individual considering the check-ins as points in the individual's trajectories.

(a)				
user_id	location_id	UTC time	timezone	
⋮	⋮	⋮	⋮	⋮
268846	42872fd9b60caeb	Tue Apr 03 18:27:37 2012	-240	
377500	3c38c65be1b8c04	Tue Apr 03 18:27:38 2012	-240	
248657	1855f964a520be3	Tue Apr 03 18:27:38 2012	-240	
⋮	⋮	⋮	⋮	⋮
(b)				
location_id	latitude	longitude	category	cc
⋮	⋮	⋮	⋮	⋮
42872fd9b60caeb	41.660393	-83.615227	College Cafeteria	US
6200f964a520ee3	40.722206	-73.981720	Theater	US
9cadf964a521fe3	44.972814	-93.235313	Student Center	US
⋮	⋮	⋮	⋮	⋮

Table 1 An example of records for the dataset D_{FS} (a) and the lookup dataset D_{loc} (b), In D_{loc} the `location_id` is associated with the coordinates, the category and the country code.

We create the mobility dataset $D_{NYC} \subset D_{FS}$ relative at the area of New York City performing a join between D_{FS} and D_{loc} on the attribute `location_id`, obtaining all the displacements made by the individuals in New York City, associated with the relative coordinates. Before performing the join, we apply some filters to obtain only the check-ins in NYC and to reduce the number of records in D_{FS} and D_{loc} , avoiding a computationally expensive operation. The resulting dataset $D_{FS,loc}$ is composed of 925,289 check-ins relative to 80,146 users. After converting the UTC in the time of New York City, we remove all the users not included in the snapshot of the social graph G scraped from Twitter. Of the 80,146 users only 8,452 appear in G (10.5%). In the next filter operation, we take only the check-ins of the 8,452 users performed during a period of three months, from April 2012 to July 2012, in this period of observation the check-ins made by the filtered users are 80,032. Then, we substitute the fast check-ins, defined as a set of check-ins such that the time difference between them is less or equal than $t = 7s$, with a single check-in where the coordinates and timestamp are the averages of the respective attributes for the *fast check-ins*. Then, we select only the users with mobility (at least two check-ins) and the users who appear in at least one edge with another of the filtered users. After the latter filtering operations, the users left are 1,780. We removed the users not in the main component of the social graph G (considering only the edges between the 1,780 users). The final dataset, D_{NYC} , contains 37,489 check-ins made

by 1,001 connected users during an observation period of three months (April 2012 to July 2012).

We analyzed the probability density functions (PDF) of the measures presented in Section 4.1, to check whether or not the obtained trajectories $\in D_{NYC}$ present the significant analytical proprieties of individuals' displacement. The distribution of the number of check-ins per user is heavy-tailed (Figure 6). This behavior is typical of the LBSN datasets [22]. The movements of the individuals in New York City are not highly predictable, as attested by the uncorrelated entropy measure (Figure 6).

The jump length confirms the tendency of individuals to move at small rather than long distances [12, 4], as we can see from Figure 6(c) individuals in the area of NYC move rarely at distances greater than ≈ 22 km. The distribution of the radius of gyration (Figure 6(d)) shows that the typical spatial spread of individuals' displacements is likely to be included between 1 and 7 km.

The probability for an individual to visit a location of rank i (Figure 6(a)), namely the location frequency, follows a distinctive distribution of this measure, the Zipf law [4]. The number of visits per each location, which correspond to the relevance of a tessellation, results in a power-law distribution (Figure 6(f)); most locations have a few visits while only rare locations receive a significant number of visits [2]. Figure 5 shows a heatmap of the check-ins $\in D_{NYC}$.

The distribution of the time spent in a location, for the 1,001 individuals, during the three months follows a power law [2, 14] (Figure 7). Humans' actions follow a circadian rhythm [2, 14]: the activity per hour measures, depicts the non-uniform distribution of the movements of individuals during the hours of a day (Figure 7).

We compute the mobility similarity for the users connected in G and for a random graph with the same number of nodes and edges. As Figure 7(c) shows, the mobility similarity within users connected in the social graph is generally higher than the ones of random pairs of users. This result confirms the correlation between human mobility and sociality: the movements of friends are more similar than those of strangers [16, 20, 15, 21].

4.4 Social Graph

The social graph G , a snapshot relative to March 2012 of the social connections among a subset of the users in D_{FS} , obtained from Twitter, is composed of 114,324 nodes and 363,704 edges. During the data preprocessing, we filter G several times, obtaining a new graph G_{NYC} (Figure 8); it is an undirected and connected graph, with 1,001 nodes which represent the users and 1,755 edges which represent the social connections between users. The graph's statistical properties follow the well-know significant properties of social graphs; the node degree distribution follows a power-law, and the average path length is 5.154 (≈ 6 in social graphs according to Karamshuk et al. [14]). The density and average node degree are respectively $4 \cdot 10^{-3}$ and 3.506.

4.5 Weighted Spatial Tessellation

To partition the area of New York City into a discrete number of relevant and *non-overlapped* locations, we used a weighted spatial *squared* tessellation L . The first consideration is that some of the locations are in the water area of New York City

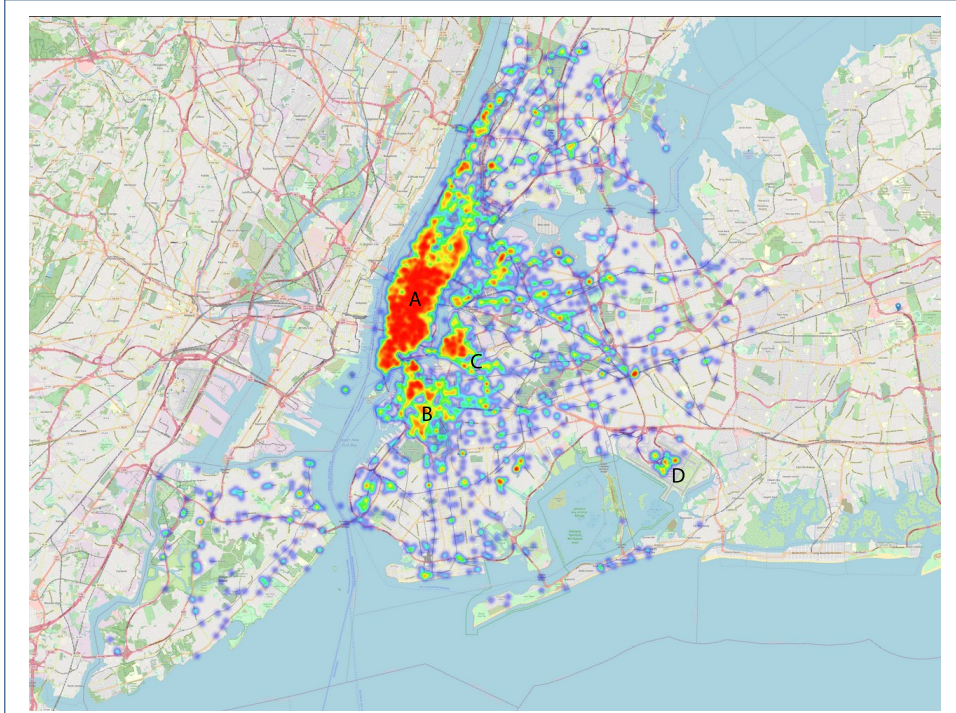


Figure 5 The heatmap relative to the 37,489 check-ins made by 1,001 individuals during an observation period of three months (April 2012 to July 2012) in New York City. There is a high concentration of check-ins in the borough of Manhattan (A) and in its surroundings (upper part of Brooklyn (B) and of Queens (C)); this high concentration of check-ins in that area can be explained mainly because Manhattan is the most densely populated of the five boroughs of New York City; another reason is that Manhattan is the touristic center of New York City, it contains attractive locations such as Times Square, Central Park, the Empire State Build, Statue of Liberty, Wall Street, One World Trade Center, and many others. Another area of dense check-ins is the one that is associated to the JFK airport (D). The distribution of the check-ins in the physical space can be considered as a continuous and non-aggregated form of relevance, from the moment that the relevance of a location is computed as the number of check-ins made in that location.

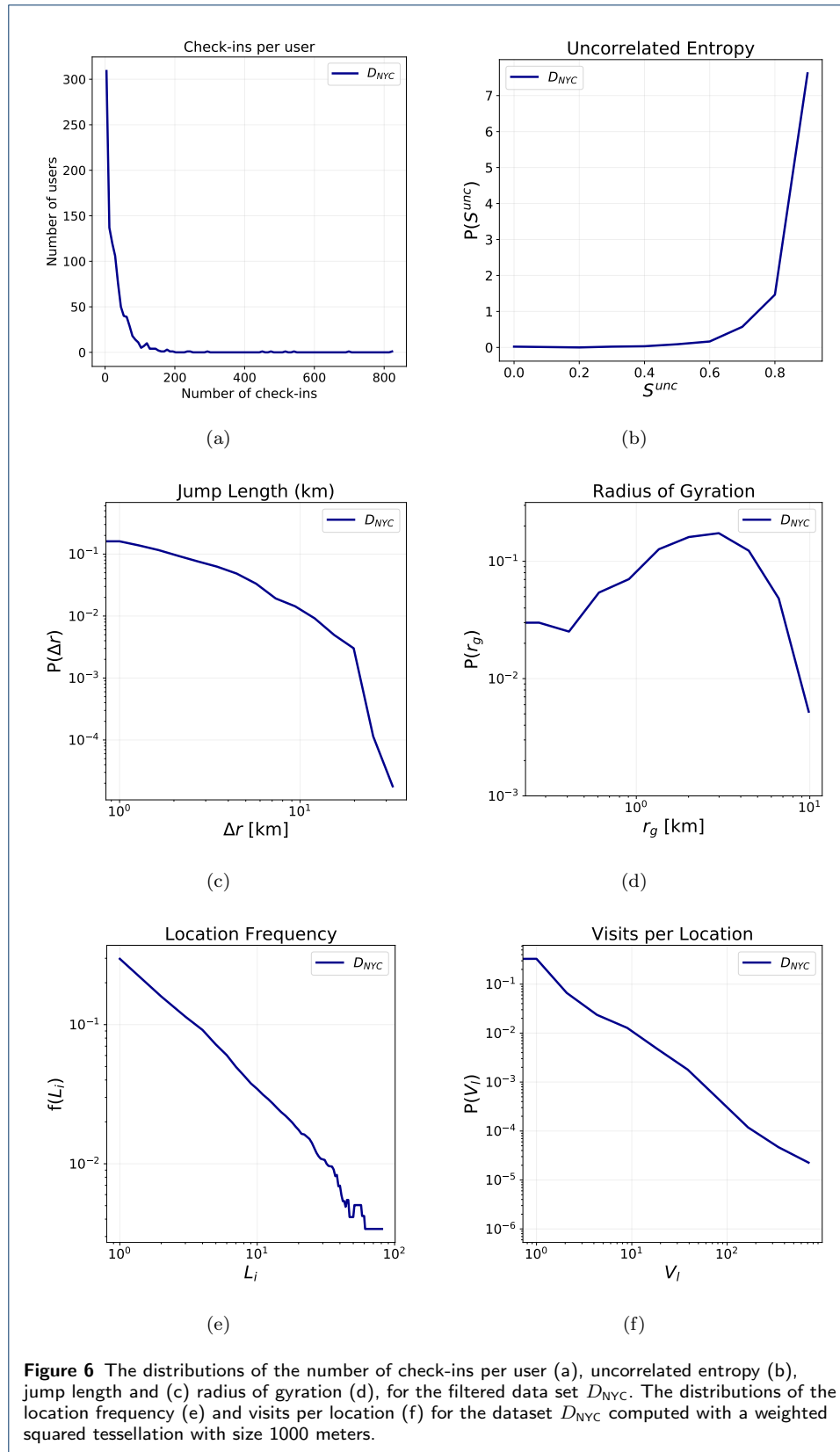
and, consequently, they are unreachable for the agents in our models. We exclude these locations obtaining a new tessellation $L_{\text{LAND}} \subseteq L$ since we consider only displacements within land locations. We compute the relevance w_i of each location $r_i \in L_{\text{LAND}}$ as the total number of check-ins in D_{NYC} made in that location by the individuals; we assigned a default relevance of 0.1 at the locations without any associated check-in. We compute another subset of locations, $L_{\text{REL}} \subseteq L_{\text{LAND}}$ defined as follows:

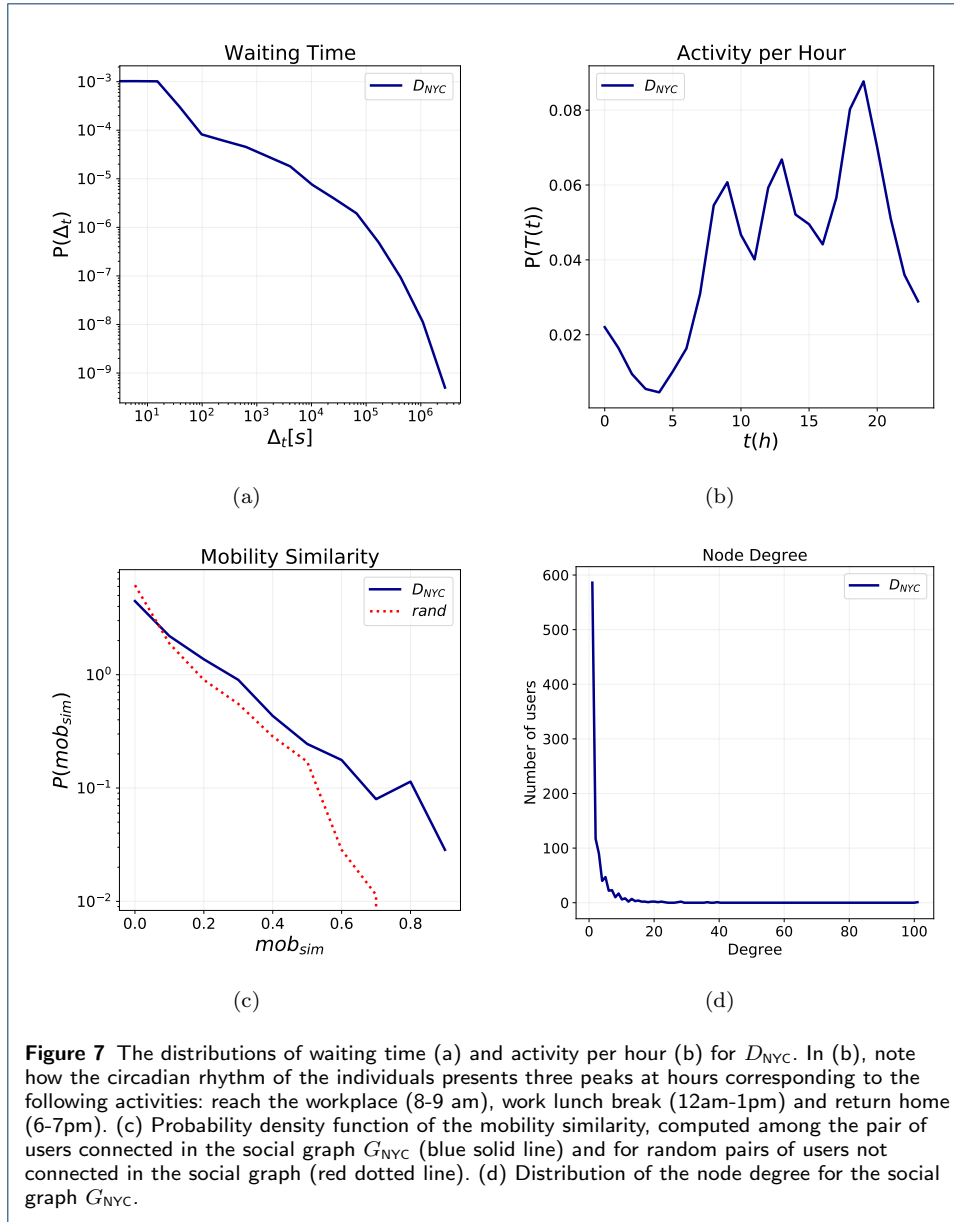
$$L_{\text{REL}} = \{r_i \in L_{\text{LAND}} \mid w_i \geq 1\} \quad (17)$$

We build the tessellations L_{LAND} and L_{REL} for different levels of granularity, we select the side s , in meters, of the squared tiles from the set $\{250, 500, 750, 1000, 2000\}$; a tessellation with locations of side s is referred as $L_{\text{LAND}}(s)$ or $L_{\text{REL}}(s)$. Table 2 shows the number of locations in each tessellation.

4.6 Experimental settings

We generate the synthetic trajectories simulating for three months the displacements of 1,001 individuals connected in the graph G_{NYC} , moving in the urban





area of New York City, represented through the tessellation L_{REL} presented in Section 4.5. During the experiments, we compare the trajectories generated by STS-EPR with the ones generated from GeoSim and two extensions of it: $GeoSim_d$ and $GeoSim_{gravity}$. In the first proposed extension, $GeoSim_d$, we introduce into GeoSim a mechanism that takes into account the distance from the current location and the location to explore. In the second extension, $GeoSim_{gravity}$, we take into account the relevance of a location together with the distance from the current location using a gravity-law. More information and technical details on the proposed extensions can be found in the Appendix. Each of the proposed extensions is instantiated with the

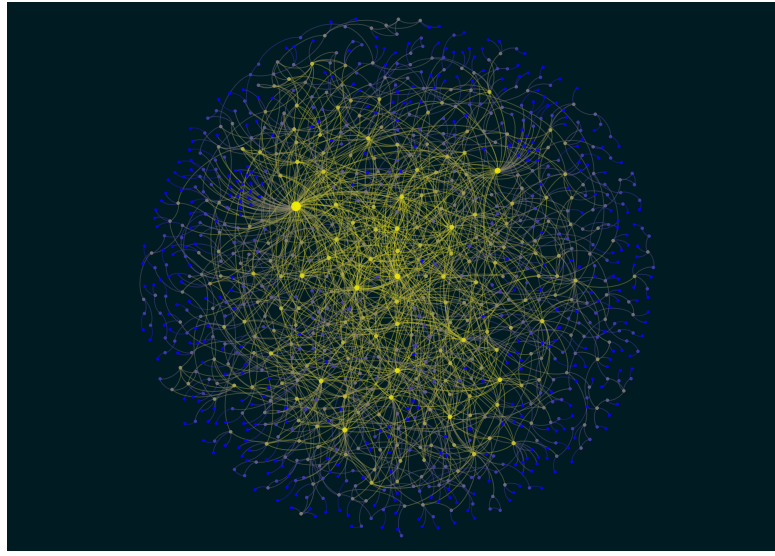


Figure 8 A visualization of the social graph G_{NYC} . The size of a node is proportional to the degree, as well as the color that varies from purple to yellow.

tile size	$ L $	$ L_{\text{LAND}} $	$ L_{\text{REL}} $
250 m	34,408	23,740	2,893
500 m	8,745	6,285	1,604
750 m	3,951	2,918	1,082
1000 m	2,256	1,709	800
2000 m	596	475	333

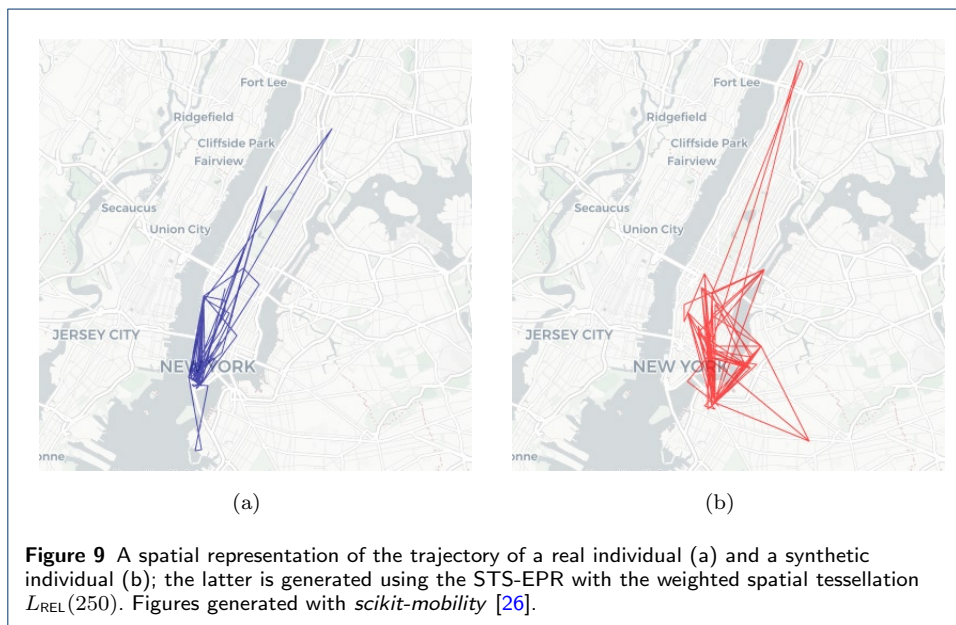
Table 2 The number of locations for each tile size for the tessellation L , L_{LAND} and L_{REL} .

additional features RSL and the action correction phase^[2]. The Markov model of STS-EPR, relative to the mobility diary generator, is trained on the displacements of the individuals included in the dataset D_{NYC} . For each model we use the weighted spatial tessellations L_{REL} for different levels of granularity, we select the side s in meters from the set $\{250, 500, 750, 1000, 2000\}$. In the experimental phase, for each model and for each tessellation we make five executions, to collect the mean and the standard deviation for each mobility measure, resulting from the comparison of the synthetic trajectories with the trajectories of real individuals.

The experiments show that the role of both the model mechanisms and the tessellation granularity is crucial to produce realistic trajectories. The probability density function of the spatial measures computed over the generated trajectories, shapes according to the mechanism used in the generative model. For what concerns the jump length (Figure 10), in GeoSim, no mechanism takes into account the spatial distance between locations, consequently, the model can not even replicate correctly the monotonicity of the distribution. In GeoSim_d, with the introduction of a mechanism that models the spatial distance between locations, the probability density function of the jump length follows the power-law behavior; the tendency of the individuals to move at small rather than long distances is preserved. How-

^[2]We tried to include also the other additional features during the experiments, namely reachable locations and social choice by degree, but they did not improve the performance of the generative models.

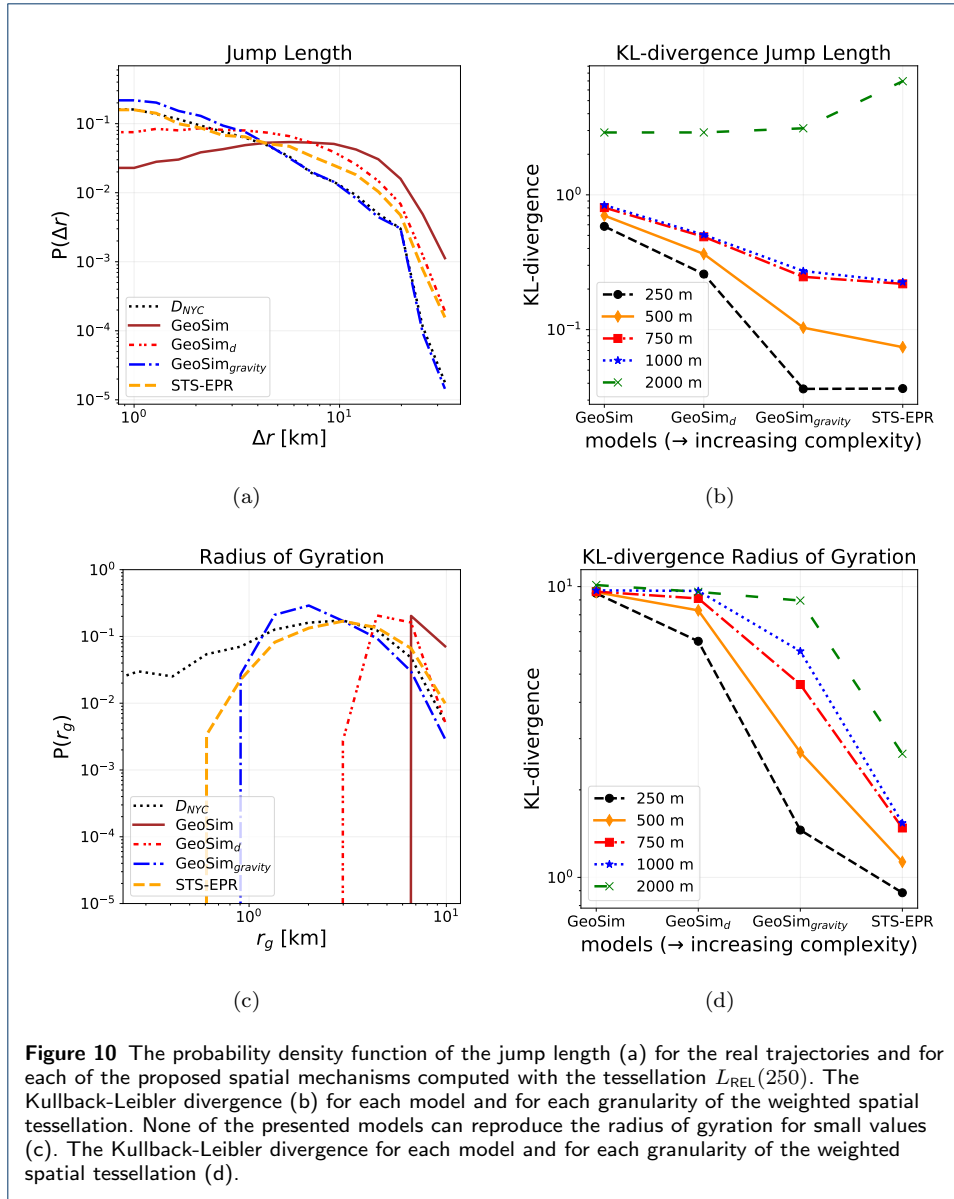
ever, taking into account only the distance is not sufficient, GeoSim_d underestimates small-distance trips and overestimates long-distance trips. With the introduction of the gravity model, $\text{GeoSim}_{gravity}$ generates trajectories that reproduce the distribution of distances accurately, although slightly overestimating small displacements. To reproduce the jump length distribution accurately, as shown in Figure 10, the granularity of the tessellation plays a crucial role together with the mechanism used in the generative model. With a fine-grained weighted spatial tessellation, the model generates more realistic trajectories (Figure 9 shows a real and a synthetic trajectory).



The considerations made for the jump length also hold for the radius of gyration; the typical spatial spread of the agents is mechanism and tessellation dependent (Figure 10). With every introduction of a more sophisticated mechanism the models generate more realistic synthetic trajectories. STS-EPR produces the most accurate trajectories, outperforming $\text{GeoSim}_{gravity}$ in terms of Kullback-Leibler divergence despite both use the gravity law. This can be due to the fact that the number of check-ins per user using the diary generator is similar to the real ones, while the other models overestimate this measure, as shown in Figure 14(a). None of the proposed models are able to reproduce correctly the radius of gyration for values smaller than $1km$.

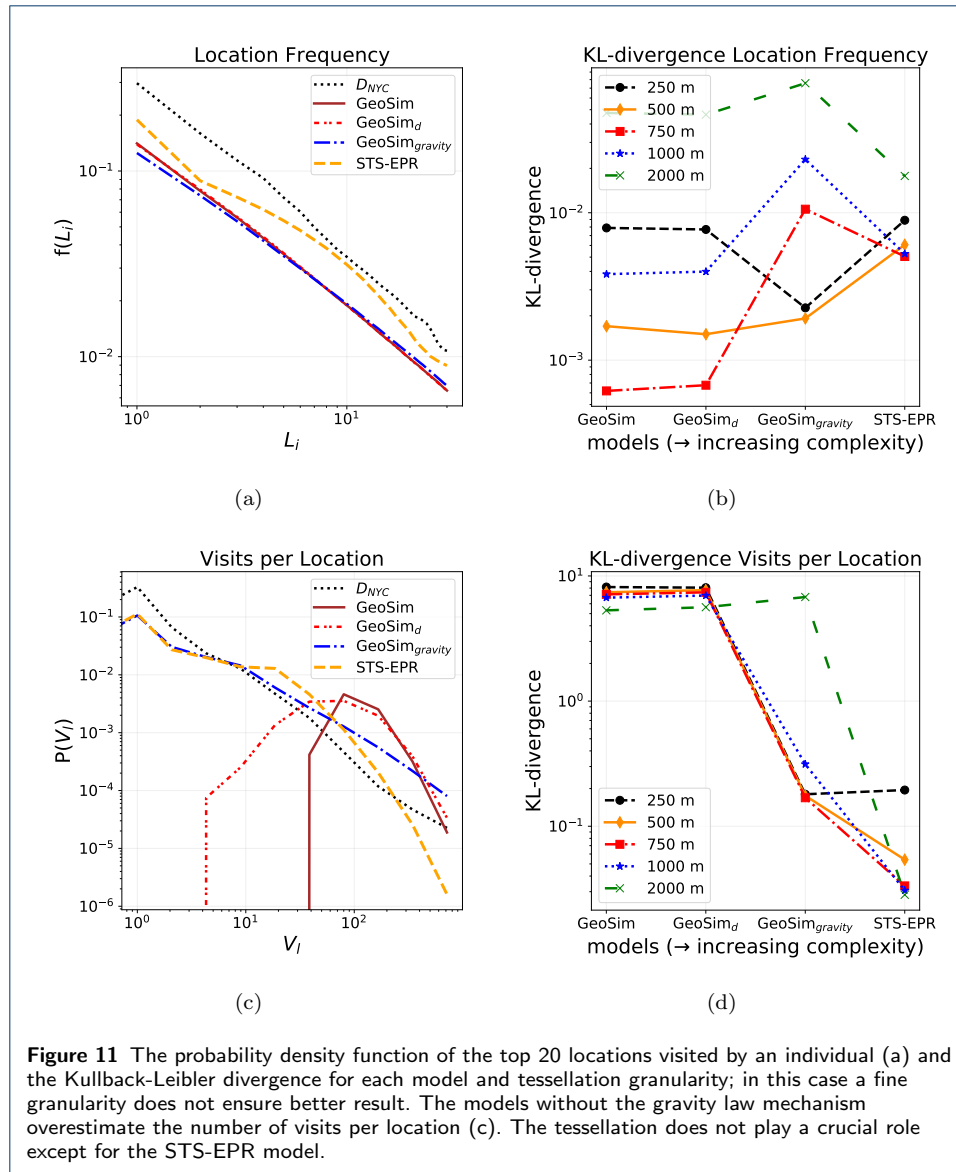
The location frequency distribution of the real data is better reproduced by STS-EPR (Figure 11(a)); STS-EPR underestimates the location frequency of the top ten locations visited by the individuals. For this measure the use of the fine-grained tessellation does not ensure better results; all the weighted spatial tessellation with size $\leq 1000 m$ produce good result in terms of KL-divergence (order of 10^{-3} for different models) as shown by the plot in Figure 11(b).

The distribution of the visits per location, equivalent at the relevance of each location, for the generated trajectories changes according to the individual exploration mechanism used in the model. The introduction of more sophisticated mechanisms produces trajectories with a more realistic number of visits per location.



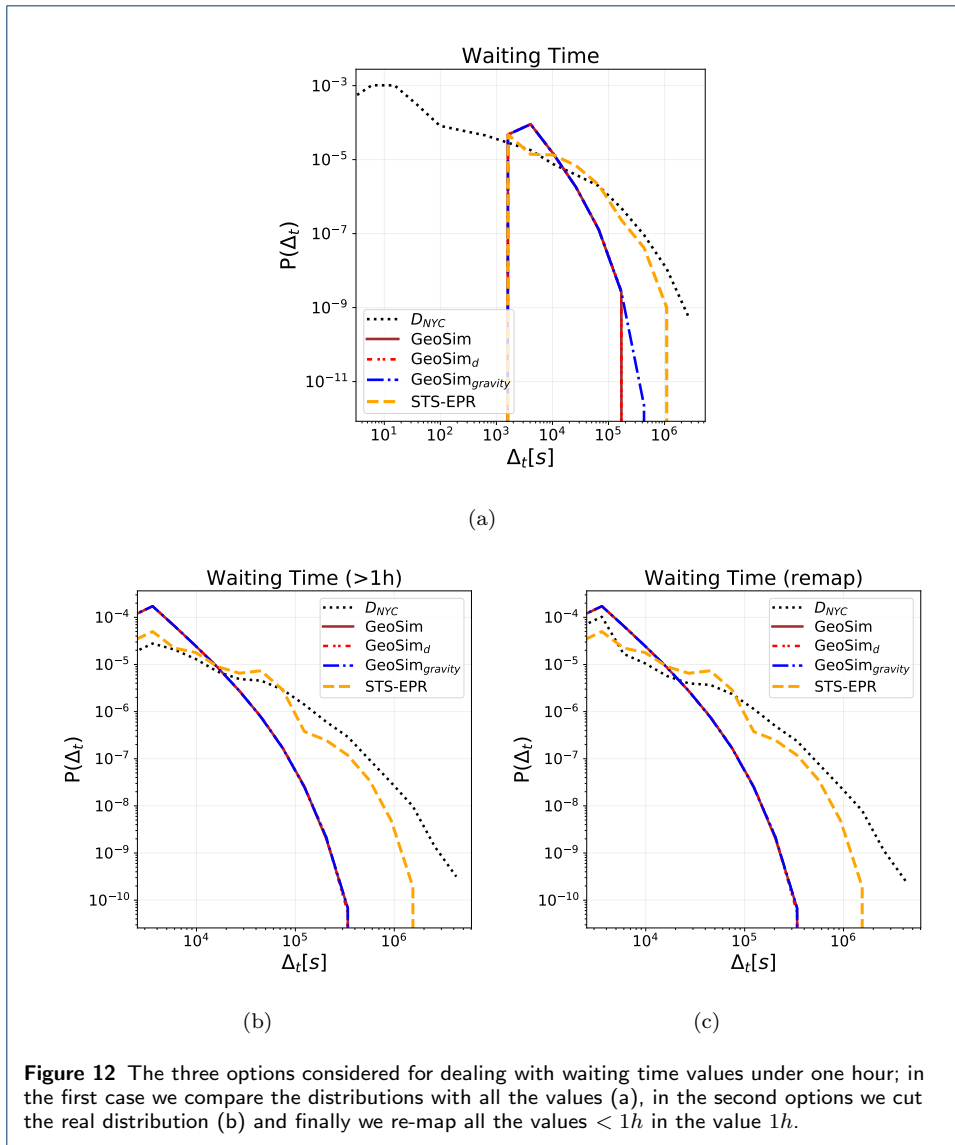
Both GeoSim and GeoSim_d underestimate the number of locations with less than 30 and 50 visits respectively (Figure 11(c)). With the introduction of the gravity law and the concept of relevance, GeoSim_{gravity} and STS-EPR replicates accurately the power-law behavior of the number of visits per location. The choice of the spatial partition is crucial for the number of visits; for the baseline model as well as GeoSim_d and GeoSim_{gravity} the tessellation used does not play a crucial role: all the tessellation with granularity $\leq 1000m$ produce similar results. In STS-EPR the results are better with a tessellation $> 250m$ because the agents perform a small number of displacement. Consequently, an aggregated number of visits considering larger locations are more similar to the real one.

The time spent in a location, namely the waiting time, has a minimum temporal resolution of one hour for the proposed model, since $min_{wt} = 1$. Since in the real distribution of the waiting time, there are values $< 1h$, to compare the synthetic and



the real distributions we consider three cases: (i) we compare the distributions as we do with the other measures (Figure 12(a)); (ii) we cut from the real distribution the waiting times $< 1h$ (Figure 12(b)); and (iii) we map all the values $< 1h$ in $1h$, preserving the number of points in the distribution (Figure 12(c)). All the models that assign the waiting time using the empirical distribution computed by Song et al. [3] behave in the same way, while the model with use the diary generator is able to reproduce more accurately the characteristic waiting time of the set of individuals in New York City.

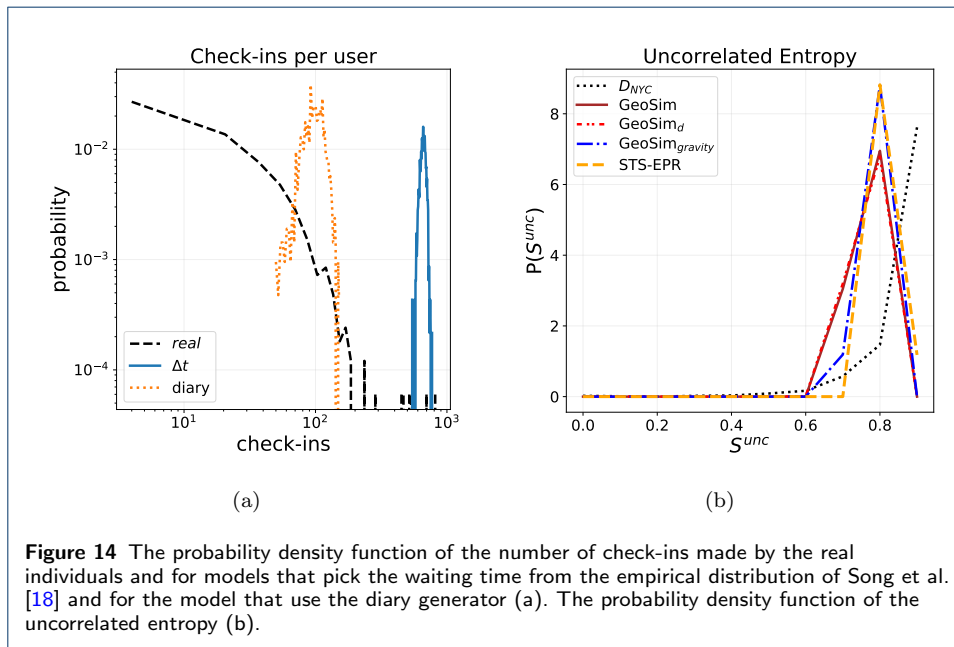
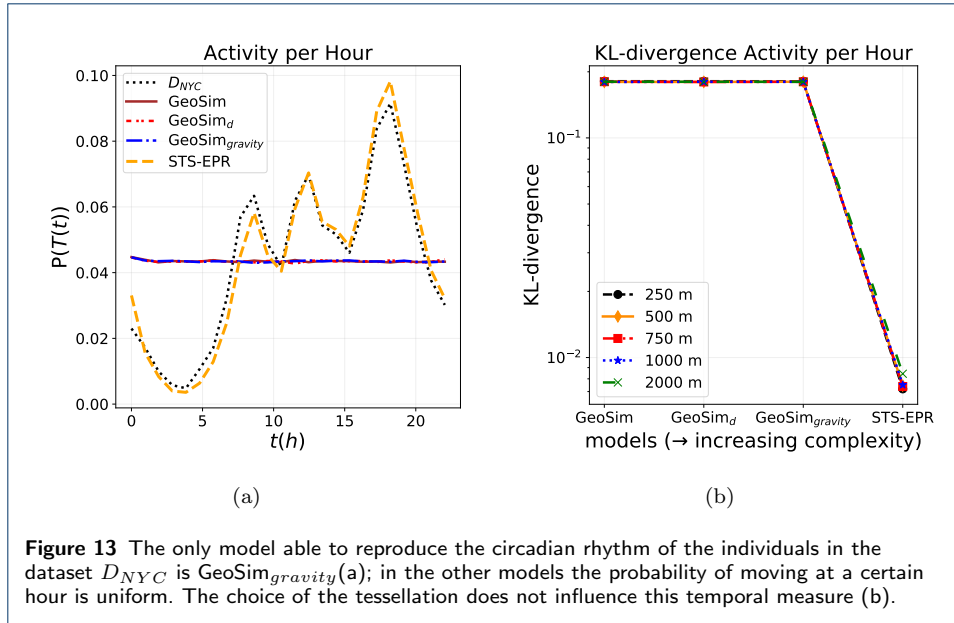
The number of trips made at each hour of the day, namely the activity per hour, depicts the tendency of individuals to move at a certain hour of the day. This measure is affected only by the time of the movements of individuals and neither by the mechanism on which they choose the next location to explore nor by the spatial tessellation used during the experiments. As we can see in Figure 13(b), the



models produce the same results with every tessellation, and the only model able to reproduce the circadian rhythm of the individuals is STS-EPR. This is caused by the fact that STS-EPR takes into account the preference of individuals to move at specific times, while GeoSim, GeoSim_d and GeoSim_{gravity} takes into account only the waiting times, without considering the hour of the day nor the preference of an individual.

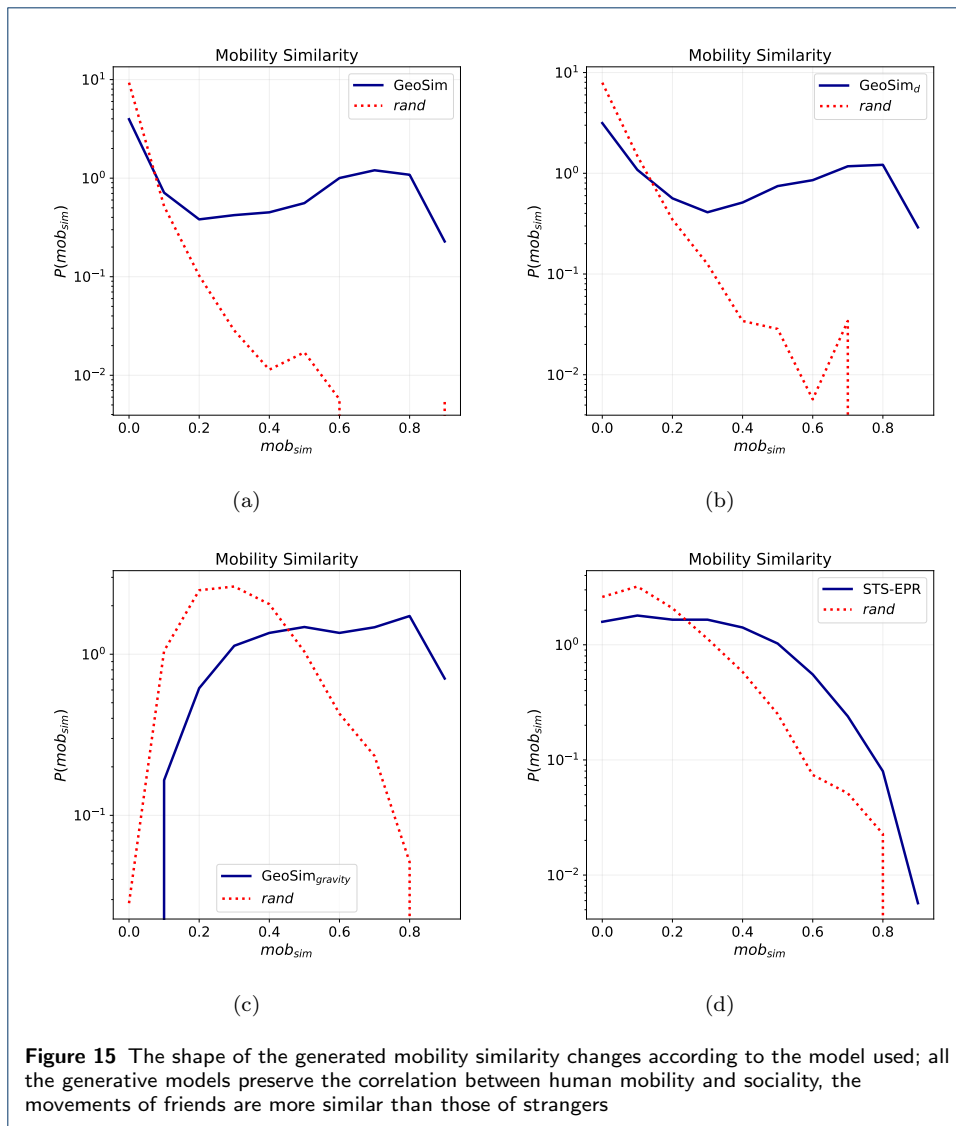
The behavior of the synthetic agents is slightly more predictable than the real counterparts; this can be caused by the fact that in the presented models, a fraction α (the social factor) of the displacements of an agent are based on the previous movements of its social contacts; this can increase the predictability of the movements of the agents. The model that reproduces in a more similar way this characteristic is STS-EPR.

The probability density function of the mobility similarity changes according to the used model; as we can see from Figure 15, the baseline model and GeoSim_d



produces similar shapes: the users connected in the graph G_{NYC} have higher mobility similarity than random pairs of non connected users. The correlation between mobility and sociality also holds for the trajectories produced by $GeoSim_{gravity}$ and STS-EPR; the model that reproduces the mobility similarity more accurately is STS-EPR (Figure 15(d)). Except for the models that does not use the gravity law, the fine-grained tessellations produce better results (Figure 16(b)).

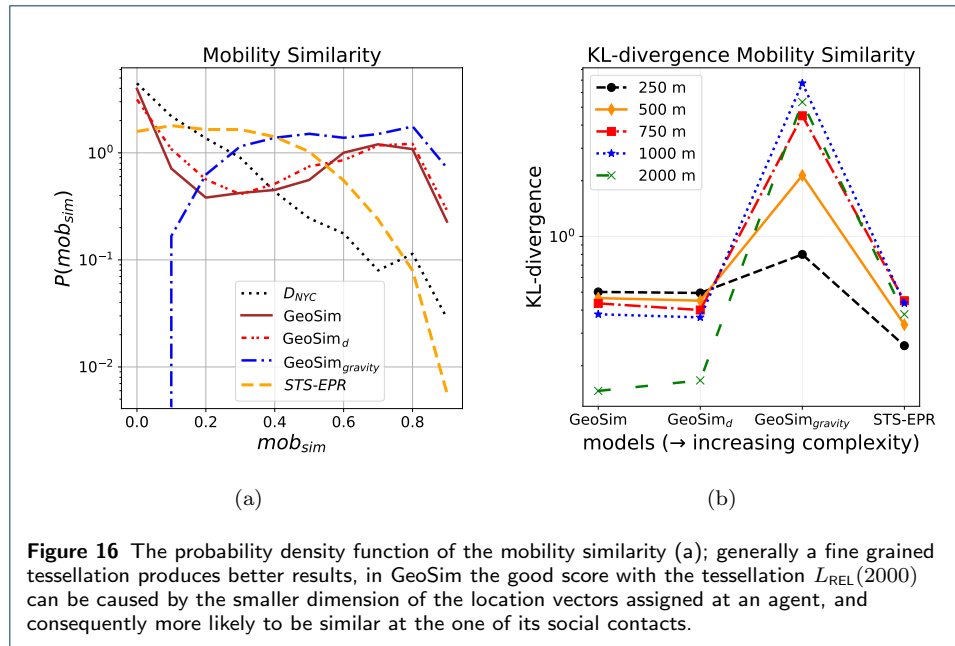
Our experiments reveal three main results. First, the proposed extension STS-EPR produces synthetic trajectories having in general the best fit to the trajectories in the dataset D_{NYC} . Second result is that the choice of the spatial mechanism and the temporal mechanism (empirical distribution or diary generator) used for picking



the waiting time is important in order to reproduce accurately some properties of the mobility trajectories; in general the gravity-law is the crucial mechanism for reproducing correctly almost all the measure. Last, the choice of the granularity of the weighted spatial tessellation depends on which measure we consider: for spatial measures (jump length and radius of gyration) as well as for the location frequency and mobility similarity a fine tessellation produces better results. In contrast, for the other measures a larger tessellation produces better trajectories.

4.7 Summary of Results

For each mobility measure we report the table of the scores obtained through the experiments, referred at the tessellation which gives the best overall result for that specific measure in terms of the five scores used to quantify the similarity between the real and the synthetic distributions. For each score, we report mean and standard deviation, the best values for each score are reported in bold.



Jump Length. The following table summarizes the scores for the jump length, using a tessellation $L_{REL}(250)$. The best models are the ones that use the gravity-law mechanism in the choice of the next location to explore.

	GeoSim	GeoSim _d	GeoSim _{gravity}	STS-EPR
RMSE	0.1044±0.0002	0.0821±0.0004	0.0364±0.0006	0.0371±0.001
KL	0.5838±0.0052	0.2583±0.004	0.0363±0.0014	0.0366±0.0016
Hellinger	0.4298±0.0009	0.2783±0.0024	0.1149±0.0032	0.1114±0.004
spearman	0.3412±0.0213	0.9594±0.0183	1.0±0.0	1.0±0.0
pearson	0.2934±0.0132	0.7201±0.0048	0.9366±0.0018	0.9787±0.0031

Table 3 Scores of the jump length measure.

Radius of Gyration. The scores reflect the fact that all the proposed models are not able to reproduce small radii correctly (Figure 10). The most accurate model is STS-EPR, the latter is the only model able to reduce in a significant way the Kullback-Leibler divergence and the Hellinger-distance score.

	GeoSim	GeoSim _d	GeoSim _{gravity}	STS-EPR
RMSE	0.1064±0.0004	0.0957±0.0003	0.0627±0.0065	0.0345±0.0044
KL	9.481±0.411	6.4871±0.0229	1.4549±0.0442	0.8855±0.2103
Hellinger	0.6507±0.0031	0.5645±0.0011	0.2977±0.0136	0.2446±0.0112
spearman	-0.3256±0.05	0.0842±0.0	0.8281±0.0	0.8299±0.0208
pearson	-0.2666±0.0057	0.1402±0.0122	0.8613±0.017	0.8826±0.0361

Table 4 Scores of the radius of gyration measure; the considered spatial tessellation is $L_{REL}(250)$.

Location Frequency. For this measure the tessellation considered is $L_{REL}(250)$; all the models are good in terms of Kullback-Leibler divergence, the only model able to reduce the Hellinger-distance is STS-EPR.

	GeoSim	GeoSim _d	GeoSim _{gravity}	STS-EPR
RMSE	0.0254±0.0002	0.0256±0.0002	0.0279±0.0001	0.0139±0.0002
KL	0.0079±0.0005	0.0077±0.0005	0.0023±0.0001	0.0089±0.0001
Hellinger	0.219±0.0005	0.2195±0.0003	0.2232±0.0002	0.1175±0.0005
spearman	1.0±0.0	1.0±0.0	1.0±0.0	1.0±0.0
pearson	0.9991±0.0002	0.9993±0.0002	0.9992±0.0003	0.9943±0.0003

Table 5 Scores for the location frequency measure, the spatial tessellation considered is $L_{REL}(250)$.

Visits per Location. From the scores (Table 6) emerges the overestimation of both GeoSim and GeoSim_d (Kullback-Leibler of 7.7095 and 6.9719 respectively) in the number of visits per location. The introduction of the concept of relevance and the mechanism of the gravity-law give the best scores.

	GeoSim	GeoSim _d	GeoSim _{gravity}	STS-EPR
RMSE	0.1013±0.0	0.1013±0.0	0.0869±0.0008	0.0464±0.0025
KL	6.7095±0.0067	6.9719±0.0137	0.3135±0.024	0.0307±0.0052
Hellinger	0.4674±0.0	0.4674±0.0	0.2696±0.0047	0.1187±0.0055
spearman	-0.5267±0.0286	-0.5965±0.0196	1.0±0.0	0.9982±0.0036
pearson	-0.1955±0.0011	-0.2276±0.0066	0.8856±0.0166	0.9976±0.0014

Table 6 Scores for the visits per location measure, the spatial tessellation considered is $L_{REL}(1000)$.

Waiting Time(s). From the three tables below we can see how the scores changes according to the distribution of the waiting time considered; considering also values $1 < h$ (Table 7) no model is able to reproduce correctly the real distribution, cutting from the real distribution all the waiting times $1 < h$ (Table 8) or remapping to an hour (Table 9) produce better scores; the model that best fits this measure is STS-EPR.

	GeoSim	GeoSim _d	GeoSim _{gravity}	STS-EPR
RMSE	0.0004±0.0	0.0004±0.0	0.0004±0.0	0.0004±0.0
KL	3.6461±0.0008	3.6405±0.0008	3.642±0.0025	2.9627±0.0057
Hellinger	0.0344±0.0	0.0344±0.0	0.0344±0.0	0.0341±0.0
spearman	0.1588±0.0	0.2658±0.0	0.2444±0.0428	0.322±0.0655
pearson	-0.1667±0.0001	-0.1653±0.0001	-0.1655±0.0006	-0.1779±0.0022

Table 7 Scores for the waiting time distribution.

	GeoSim	GeoSim _d	GeoSim _{gravity}	STS-EPR
RMSE	0.0±0.0	0.0±0.0	0.0±0.0	0.0±0.0
KL	0.5619±0.0011	0.5609±0.0003	0.5644±0.0027	0.0423±0.0031
Hellinger	0.0065±0.0	0.0065±0.0	0.0065±0.0	0.0014±0.0001
spearman	0.5179±0.0	0.5179±0.0	0.5254±0.0149	0.8851±0.0281
pearson	0.9154±0.0001	0.9154±0.0002	0.9153±0.0003	0.9769±0.0009

Table 8 Scores for the waiting time distribution where are considered only values ≥ 1 hour.

	GeoSim	GeoSim _d	GeoSim _{gravity}	STS-EPR
RMSE	0.0±0.0	0.0±0.0	0.0±0.0	0.0±0.0
KL	0.1976±0.0006	0.1972±0.0004	0.198±0.0007	0.2045±0.0051
Hellinger	0.0043±0.0	0.0043±0.0	0.0042±0.0	0.0029±0.0
spearman	0.5179±0.0	0.5179±0.0	0.5254±0.0149	0.8851±0.0281
pearson	0.975±0.0001	0.9749±0.0002	0.9751±0.0001	0.9178±0.0015

Table 9 Scores for the waiting time distribution where the values ≥ 1 hour are considered as 1 hour.

Activity per Hour. The three models that use the empirical distribution of Song et al. [18] in the waiting time choice behave the same. The only model able to reproduce the circadian rhythm is STS-EPR.

	GeoSim	GeoSim _d	GeoSim _{gravity}	STS-EPR
RMSE	0.0234±0.0001	0.0234±0.0	0.0234±0.0	0.0047±0.0001
KL	0.1797±0.0007	0.1801±0.0004	0.18±0.0006	0.0075±0.0003
Hellinger	0.2268±0.0004	0.227±0.0002	0.2269±0.0004	0.0431±0.0009
spearman	-0.1078±0.2374	-0.2607±0.1109	-0.2214±0.1681	0.9786±0.0016
pearson	-0.2008±0.1717	-0.2962±0.0873	-0.2531±0.1352	0.9834±0.0006

Table 10 Scores for the activity per hour measure.

Uncorrelated Entropy. The best tessellation for this measure is $L_{REL}(2000)$; all the models are not able to reproduce in an accurate way the distribution of the uncorrelated entropy of the individuals in New York City.

	GeoSim	GeoSim _d	GeoSim _{gravity}	STS-EPR
RMSE	2.0942±0.0405	2.0842±0.0207	2.4114±0.0141	2.2734±0.0129
KL	7.3433±0.0099	7.3404±0.0048	7.4983±0.0147	3.4449±0.2474
Hellinger	1.7999±0.0085	1.7974±0.0042	1.9059±0.0078	1.7716±0.0242
spearman	0.5276±0.0	0.5276±0.0	0.5276±0.0	0.768±0.0
pearson	0.5544±0.0021	0.555±0.0011	0.5357±0.0009	0.5456±0.0014

Table 11 Scores for the uncorrelated entropy measure.

Mobility Similarity. The best model for what concern the distribution of the mobility similarity with respect the social graph G is STS-EPR. In this case the use of the gravity-law with the waiting times chosen from the empirical distribution of Song et al. [18] gives the worst result; using a diary generator and the gravity law like in STS-EPR is the best choice according to the results presented in Table 12.

	GeoSim	GeoSim _d	GeoSim _{gravity}	STS-EPR
RMSE	1.3609±0.0236	1.3677±0.021	1.904±0.0478	0.9007±0.0318
KL	0.5013±0.0085	0.495±0.007	0.7998±0.0403	0.2568±0.0238
Hellinger	1.2843±0.0091	1.2743±0.0092	1.5087±0.0284	0.7958±0.018
spearman	0.1345±0.0225	0.1879±0.0153	0.4594±0.0145	0.9222±0.0102
pearson	0.9432±0.0041	0.9517±0.0033	0.8638±0.0311	0.9785±0.0028

Table 12 The scores referred to the measure mobility similarity using a tessellation $L_{REL}(250)$.

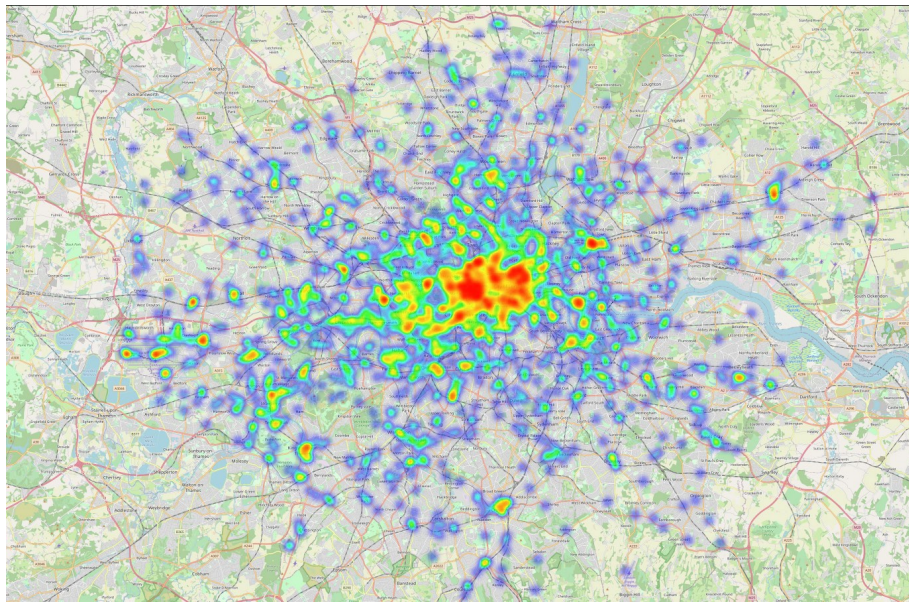


Figure 17 The heatmap relative at the 14,895 check-ins made by 622 individual during an observation period of three months (April 2012 to July 2012) in London. From the heatmap emerges an high concentration of check-ins in the borough of Westminster and City of London.

4.8 Modeling ability in new scenarios

For assessing the modeling ability of the proposed model in other scenarios beyond New York City, we simulate the mobility for a set of individuals moving in the area of London for three months. Specifically, we instantiate STS-EPR on a weighted spatial tessellation with a granularity of 250 meters. The dataset D_{LON} , relative at the mobility of the individuals in London, is created using the same *modus operandi* as for the New York City dataset D_{NYC} ; D_{LON} contains 14,895 check-ins (Figure 17) made by 622 users connected in a social graph G_{LON} which has 1,185 edges. The weighted spatial tessellation $L_{LON}(250)$ computed over D_{LON} contains 2,800 relevant locations.

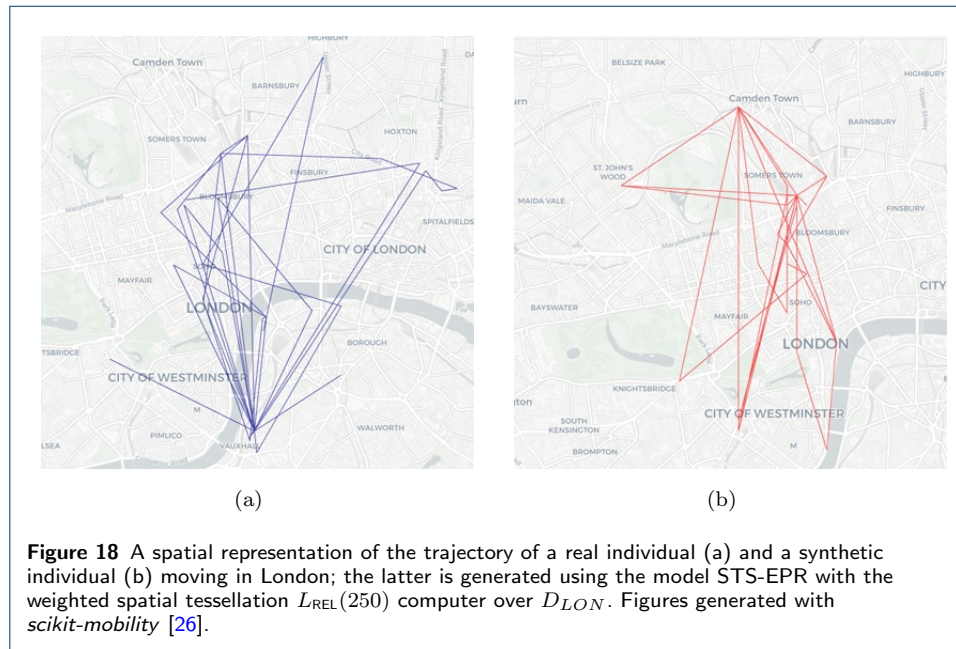
First, we verify that the model is not *city-dependent*; we instantiate the model with full knowledge of the London scenario (diary generator MD_{LON} and weighted spatial tessellation $L_{LON}(250)$); as shown in Table 13, the model is able to generate trajectories (Figure 18) with realistic mobility patterns.

Next, we simulate three scenarios where we have partial or no information about the displacements and the circadian rhythm of the individuals in London. In the first scenario (**None** scenario), we assume to know nothing about the mobility of the individuals in London. We use the Mobility Diary Generator MD_{NYC} computed for New York City, and we generate the weighted spatial tessellation assigning a relevance w_i for a location r_i from a truncated power-law $P(w) \approx (w)^{-\beta} e^{-w/\lambda}$ where $\beta = 1.25$ and $\lambda = 104$. We fit the parameters over the distribution of the relevance of the locations in New York City. In the second scenario (**MD** scenario), we assume to know only the routine of the individuals in London using the Mobility Diary Generator MD_{LON} and the weighted spatial tessellation used by the model is the one fitted on the New York's locations. In the last scenario (L_{LON} scenario),

	Δr	r_g	L_i	Vl	Δ_{tmap}	$t(h)$	S^{unc}	mob_{sim}
None	0.044	3.1222	0.0152	0.1575	0.2455	0.066	2.2479	0.2699
	0.0033	0.726	0.0006	0.0112	0.0016	0.0011	0.0779	0.02
MD	0.0345	2.3151	0.0102	0.1503	0.1656	0.0117	1.3514	0.2278
	0.0021	0.5801	0.0005	0.0123	0.0042	0.0006	0.2133	0.0167
L_{LON}	0.017	1.4486	0.0153	0.1534	0.2472	0.0655	2.1396	0.2847
	0.0025	0.3124	0.0005	0.0139	0.0039	0.0008	0.2578	0.0223
Full	0.0119	0.9861	0.0106	0.1407	0.1643	0.0113	1.3445	0.2342
	0.0008	0.4517	0.0003	0.0078	0.0045	0.001	0.2267	0.016
NYC	0.0366	0.8855	0.0089	0.1947	0.1665	0.0072	2.1176	0.2568
	0.0016	0.2103	0.0001	0.0161	0.0054	0.0003	0.3345	0.0238

Table 13 Table of the results for the experiments of individuals' mobility in London. Every of the first four rows corresponds to a different scenario described above; the last row reports the results of the experiments in New York City using the tessellation granularity of 250 meters. Every column refers to a standard mobility measure. Every cell reports the mean Kullback-Leibler score (first row) and the standard deviation (second row).

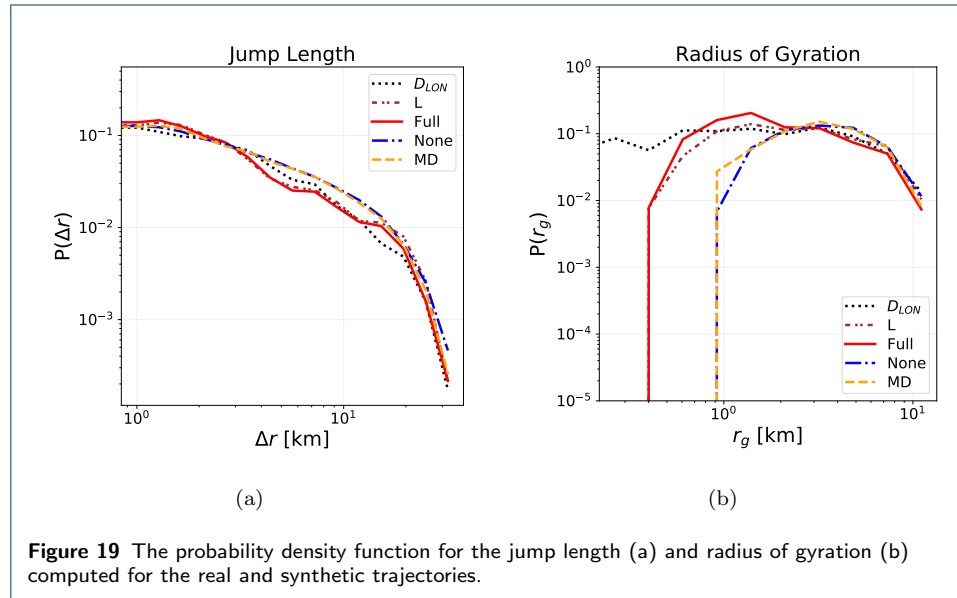
we assume to know only the real weighted spatial tessellation $L_{LON}(250)$ using the Mobility Diary Generator MD_{NYC} .



As shown in Table 13, STS-EPR reproduces the standard mobility measures accurately, with results similar to those obtained in the experiments concerning the area of New York City. The model can generate realistic trajectories, even with a lack of information. Without including neither the diary generator of the individuals in London nor the weighted spatial tessellation computed over D_{LON} (first row Table 13), the scores are in general worst than the full-knowledge scenario but still good considering that the model use no information about the mobility behavior of the individuals in London. Including in the model, in a complementary way, the real

weighted spatial tessellation and the real Mobility Diary, we obtain more realistic trajectories in terms of spatial and spatio-temporal patterns, respectively.

The model replicates the distribution of the jump length associated with the synthetic trajectories (Figure 19(a)) accurately; instead, the models cannot replicate the shape of the distribution of the radius of gyration (Figure 19(b)).



Both the measures concerning the frequency and the number of visits in each location are reproduced accurately by the synthetic trajectories; the model in the experiments which uses the Mobility Diary Generator of New York City underestimates the frequency for the first ten locations (Figure 20(a)); the same holds for the visits per location measure where is present a slightly underestimation of the number of location with a small number of visits. (Figure 20(b)).

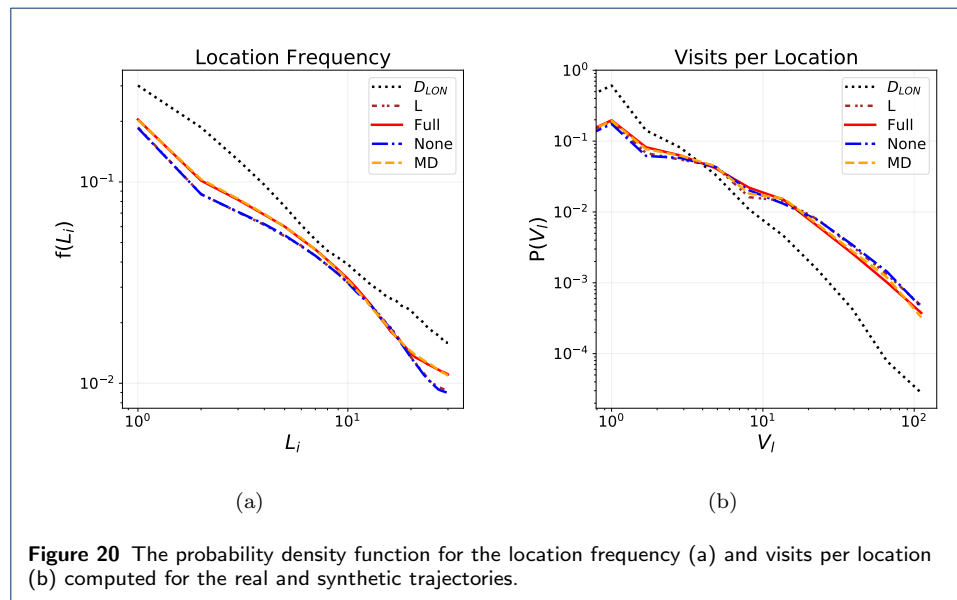
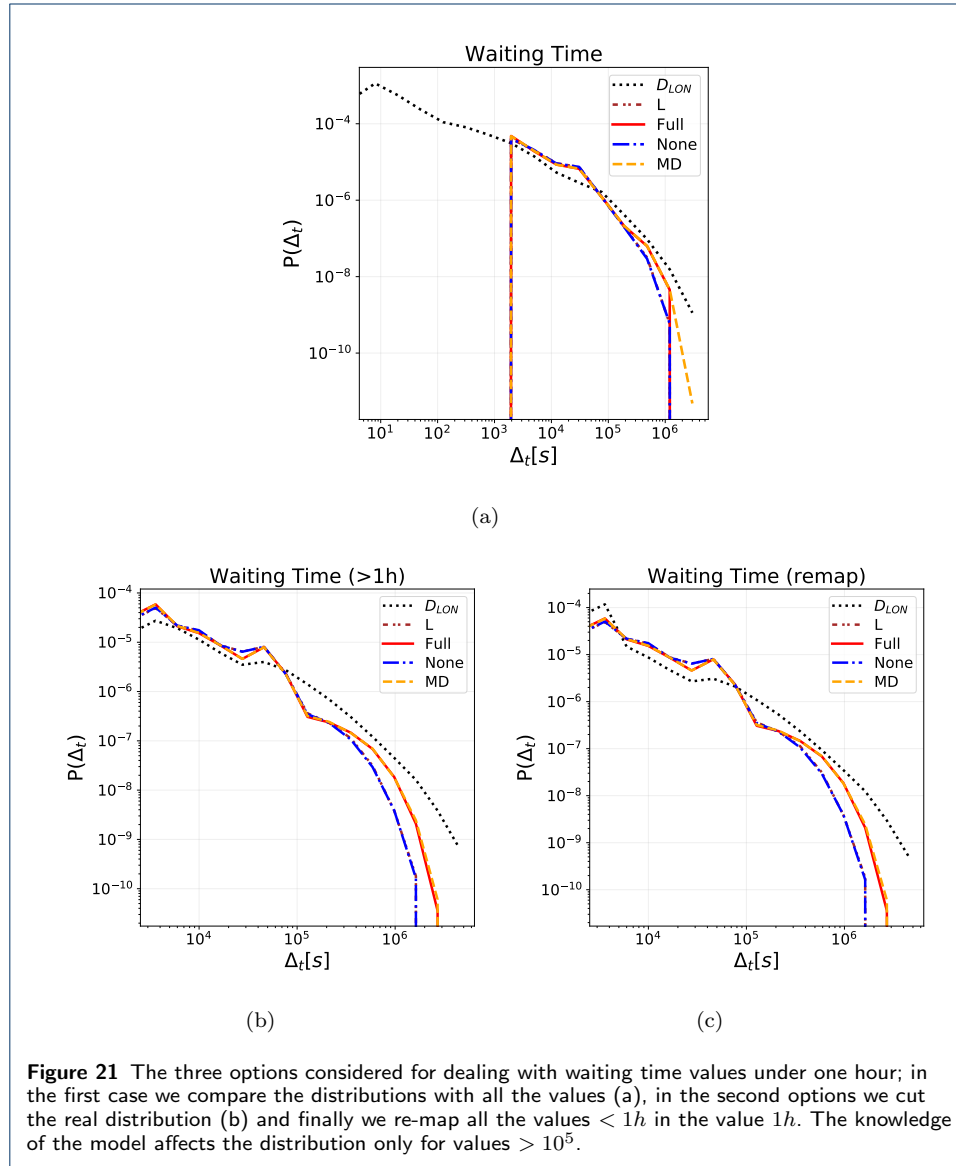
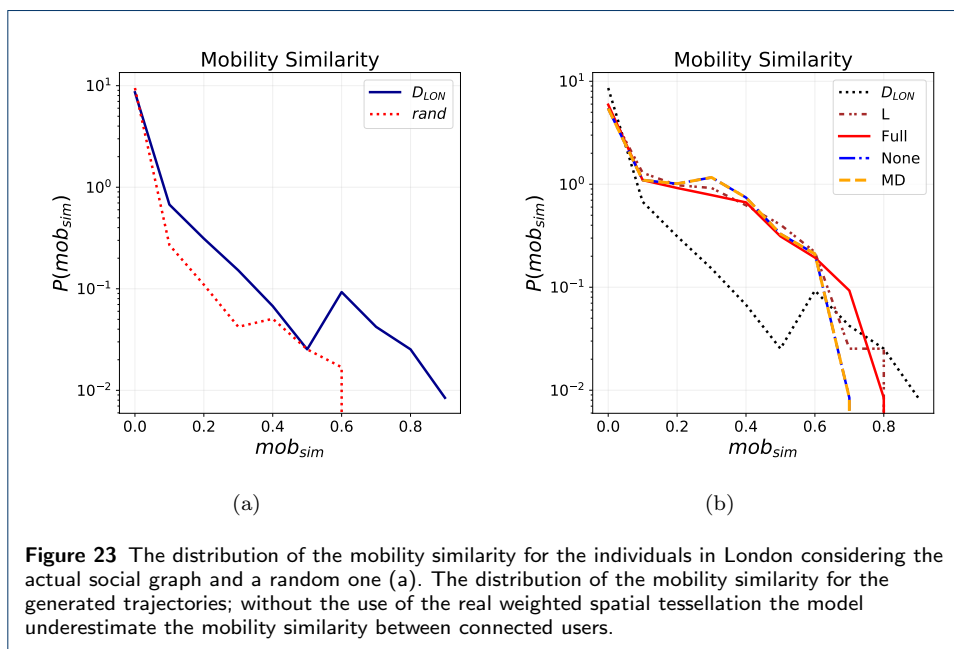
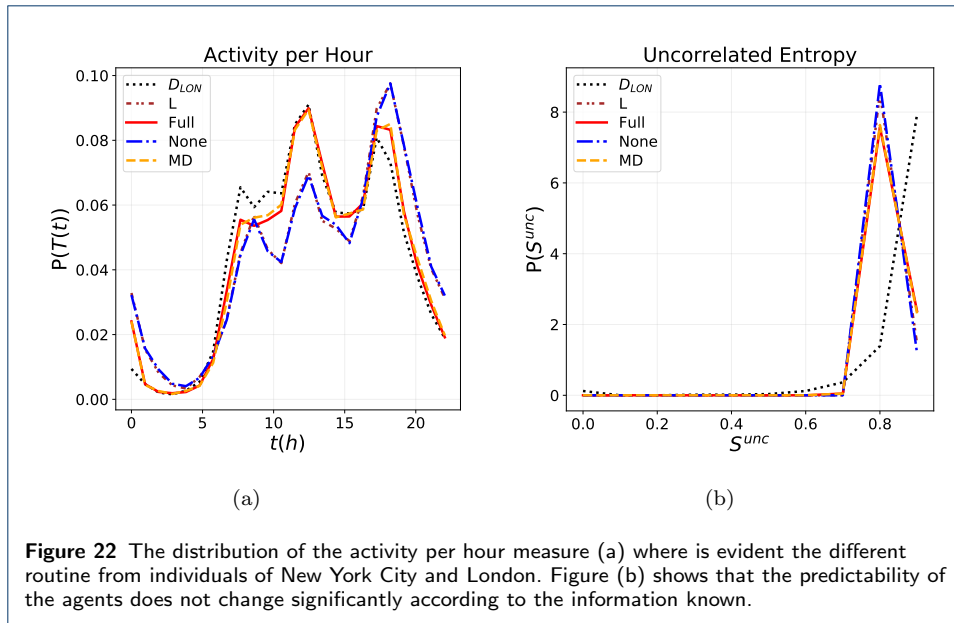


Figure 21 shows how the waiting time, in the three variants presented before, is affected by the amount of real information known by the model for values $> 10^5$. From Figure 22(a) is evident the different circadian rhythm between the individuals



in New York City and London. The circadian rhythm of the individuals in New York is characterized by three peaks, while for individuals in London, it is characterized by two peaks. This can be explained due to the different socio-cultural behaviors of the two studied populations. The predictability of the synthetic agents is not influenced by the knowledge modeled by STS-EPR (Figure 22(b)). The mobility similarity distribution between the generated trajectories of the agents, changes according to the real information included in the model (Figure 16(a)); without the use of the real weighted spatial tessellation the model underestimate the mobility similarity between connected users.

These experiments demonstrate and validate the applicability of STS-EPR in urban areas beyond New York City. It can be used in an unseen scenario using a



pre-computed Mobility Diary Generator^[3] and a weighted spatial tessellation with relevance picked from the empirical truncated-power law $P(w) \approx (w)^{-\beta} e^{-w/\lambda}$ where $\beta = 1.25$ and $\lambda = 104$.

5 Conclusions and Future Works

In this work, we develop a model that considers the social dimension and spatial and temporal dimensions during the generation of the synthetic trajectories.

^[3]A pre-computed Mobility Diary Generator is available at https://github.com/kdd-lab/2019_Cornacchia

Starting from GeoSim, we include three mobility mechanisms to improve its modeling ability: a mechanism that takes into account the distance from the current location and the location to explore; the relevance of a location together with the distance from the current location using a gravity-law; an algorithm that captures the tendency of individuals to follow or break their routine. We also include other novel additional mechanisms: the RSL (Relevance-based Starting Location) principle, which considers the relevance during the assignment of the agents at their starting location; the reachable location concept, where we model the fact that an agent, associated with waiting time, can visit only the locations reachable traveling at a certain speed for the associated amount of time; the concept of the popularity of an agent at a collective level during the contact selection phase, when an agent decides to explore a new location; and we specify how to deal with borderline cases, proposing an action correction phase.

Our experiments on 1,001 individuals connected in a social graph, moving for three months in the urban area of New York City, reveal that STS-EPR can generate realistic trajectories. Interestingly, both the mechanisms and the tessellation granularity are crucial to producing realistic trajectories. We further validate the modeling ability of STS-EPR simulating the mobility of individuals moving in London, including in the model different levels of knowledge concerning their mobility behaviors. From the results obtained, we can conclude that the model can generate realistic mobility trajectories independently from the urban area considered, and even with a lack of crucial information.

The proposed model can be further improved in several directions. The concept of spatial distance between the current location and the location to visit in the next displacement is considered only in the individual exploration; it can also be considered in the other cases together with the visitation pattern of the individual. In the proposed models, the social graph is static. An interesting improvement can be to consider a dynamic social graph where the agents can create new links. Another consideration is that, for example, during the working hours, an individual tends to interact mainly with its colleagues. In contrast, evening activities will be influenced mostly by its family or friends [14]. The social relationships of an individual change with time and the social graph can be modeled as a time-varying social graph: a graph where the weight of the connections changes according to the time and the social community of the contact. Currently, in the models, there is no representation of the urban infrastructure like urban roads. An improvement can be to consider the road network of a city and the speed limit associated with each road. In this scenario, the agent reaches its selected location traveling through the road infrastructure, respecting the speed limits associated with the roads on its path.

An interesting improvement can be to use a different weighted spatial tessellation from the squared one used during our experiments. For example, a tessellation where the tiles do not cover the same area, but rather that contains a specific amount of population. In this way, a high population area will be partitioned in many small tiles; in contrast, a low population area will be represented with a small number of large tiles. Two libraries that allow this partition of the space in hierarchical hexagon tessellation are Uber's H3^[4] and Google S2 Geometry^[5]. From the exper-

^[4]<https://eng.uber.com/h3>

^[5]<https://s2geometry.io>

iments emerges that the use of a correct Mobility Diary Generator is essential to generate realistic trajectories; as shown in Section 4.8, the circadian rhythm varies between populations to their socio-cultural tradition. Different factors can shape the circadian rhythm of a population. An interesting improvement is designing a model to generate a plausible Mobility Diary Generator, if it is not available, starting from information about a population, such as the working hours schedule, opening hours of activities (e.g., schools, restaurants, shops). Also, the relevance of the locations plays a crucial role; when information about the relevance is not available, a solution besides the use of the population density is to assign a relevance according to the empirical power-law distribution presented in Section 4.8. However, the heatmaps relative to the check-ins in New York City and London show that the relevant locations are clustered in space, and this can not be modeled using only the power-law distribution. A solution can be to create a model in which the relevance of a location is more likely to be high if it surrounded by relevant locations. Artificial Intelligence techniques, such as Generative Adversarial Networks (GANs), are used to generate synthetic trajectories that follow the distribution of real mobility trajectories used as a train dataset [27]. GANs can be embedded into the mechanistic models to produce more realistic trajectories, capturing the aspects of human movements that can not be modeled from the mechanisms of such generative models [27]. This hybrid model could represent a further step forward in modeling and understanding human mobility.

Competing interests

The authors declare that they have no competing interests.

Author's contributions

GC implemented the code, preprocessed the data, made the experiments and the plots, and wrote the article. LP supervised and directed the work, designed the experiments, selected the baseline models, and wrote the article. GR suggested experiments about the social aspect of human mobility.

Acknowledgements

This research has been partially supported by EU project H2020-INFRAIA SoBigData++ grant agreement #871042.

Author details

¹University of Pisa, Pisa, Italy. ²ISTI-CNR, Pisa, Italy.

References

- Barbosa, H., Barthelemy, M., Ghoshal, G., James, C., Lenormand, M., Louail, T., Menezes, R., Ramasco, J.J., Simini, F., Tomasini, M.: Human mobility: Models and applications. *Physics Reports* (2017). doi:[10.1016/j.physrep.2018.01.001](https://doi.org/10.1016/j.physrep.2018.01.001)
- Pappalardo, L., Simini, F.: Data-driven generation of spatio-temporal routines in human mobility. *Data Mining and Knowledge Discovery* **32** (2017). doi:[10.1007/s10618-017-0548-4](https://doi.org/10.1007/s10618-017-0548-4)
- Song, C., Koren, T., Wang, P., Barabasi, A.-L.: Modelling the scaling properties of human mobility. *Nature Physics* **6** (2010). doi:[10.1038/nphys1760](https://doi.org/10.1038/nphys1760)
- Gonzalez, M.C., Hidalgo, C., Barabasi, A.-L.: Understanding individual human mobility patterns. *Nature* **453**, 779–82 (2008). doi:[10.1038/nature06958](https://doi.org/10.1038/nature06958)
- Pappalardo, L., Barlacchi, G., Pellungrini, R., Simini, F.: Human mobility from theory to practice: data, models and applications. In: *Companion Proceedings of The 2019 World Wide Web Conference. WWW '19*, pp. 1311–1312. Association for Computing Machinery, New York, NY, USA (2019). doi:[10.1145/3308560.3320099](https://doi.org/10.1145/3308560.3320099). <https://doi.org/10.1145/3308560.3320099>
- Cintia, P., Fadda, D., Giannotti, F., Pappalardo, L., Rossetti, G., Pedreschi, D., Rinzivillo, S., Bonato, P., Fabbri, F., Penone, F., Savarese, M., Checchi, D., Chiaromonte, F., Vineis, P., Guzzetta, G., Riccardo, F., Marziano, V., Poletti, P., Trentini, F., Bella, A., Andrianou, X., Manso, M.D., Fabiani, M., Bellino, S., Boros, S., Urdiales, A.M., Vescio, M.F., Brusaferrero, S., Rezza, G., Pezzotti, P., Ajelli, M., Merler, S.: The relationship between human mobility and viral transmissibility during the COVID-19 epidemics in Italy (2020). [2006.03141](https://doi.org/10.2006.03141)
- Montjoye, Y.-A., Hidalgo, C., Verleysen, M., Blondel, V.: Unique in the crowd: The privacy bounds of human mobility. *Scientific reports* **3**, 1376 (2013). doi:[10.1038/srep01376](https://doi.org/10.1038/srep01376)
- Montjoye, Y.-A., Gams, S., Blondel, V., Canright, G., Cordes, N., Deletaille, S., Engø-Monsen, K., García-Herranz, M., Kendall, J., Kerry, C., Krings, G., Letouzé, E., Luengo-Oroz, M., Oliver, N., Rocher, L., Rutherford, A., Smoreda, Z., Steele, J., Wetter, E., Bengtsson, L.: On the privacy-conscious use of mobile phone data. *Scientific Data* **5**, 180286 (2018). doi:[10.1038/sdata.2018.286](https://doi.org/10.1038/sdata.2018.286)

9. Pellungrini, R., Pappalardo, L., Pratesi, F., Monreale, A.: A data mining approach to assess privacy risk in human mobility data. *ACM Trans. Intell. Syst. Technol.* **9**(3) (2017). doi:[10.1145/3106774](https://doi.org/10.1145/3106774)
10. Barbosa-Filho, H., Barthelemy, M., Ghoshal, G., James, C., Lenormand, M., Louail, T., Menezes, R., Ramasco, J.J., Simini, F., Tomasini, M.: Human mobility: Models and applications. *Physics Reports* **734**, 1–74 (2018)
11. Karamshuk, D., Boldrini, C., Conti, M., Passarella, A.: Human mobility models for opportunistic networks. *IEEE Communications Magazine* **49**(12), 157–165 (2011)
12. Brockmann, D., Hufnagel, L., Geisel, T.: The scaling laws of human travel. *Nature* **439**, 462–5 (2006). doi:[10.1038/nature04292](https://doi.org/10.1038/nature04292)
13. Pappalardo, L., Rinzivillo, S., Qu, Z., Pedreschi, D., Giannotti, F.: Understanding the patterns of car travel. *The European Physical Journal Special Topics* **215**(1), 61–73 (2013). doi:[10.1140/epjst/e2013-01715-5](https://doi.org/10.1140/epjst/e2013-01715-5)
14. Karamshuk, D., Boldrini, C., Conti, M., Passarella, A.: Human mobility models for opportunistic networks. *IEEE Communications Magazine* **49**, 157–165 (2011). doi:[10.1109/MCOM.2011.6094021](https://doi.org/10.1109/MCOM.2011.6094021)
15. Cho, E., Myers, S., Leskovec, J.: Friendship and mobility: User movement in location-based social networks, pp. 1082–1090 (2011). doi:[10.1145/2020408.2020579](https://doi.org/10.1145/2020408.2020579)
16. Toole, J., Herrera-Yague, C., Schneider, C., Gonzalez, M.C.: Coupling human mobility and social ties. *Journal of the Royal Society, Interface / the Royal Society* **12** (2015). doi:[10.1098/rsif.2014.1128](https://doi.org/10.1098/rsif.2014.1128)
17. Pappalardo, L., Simini, F., Rinzivillo, S., Pedreschi, D., Giannotti, F., Barabasi, A.-L.: Returners and explorers dichotomy in human mobility. *Nature Communications* **6** (2015). doi:[10.1038/ncomms9166](https://doi.org/10.1038/ncomms9166)
18. Song, C., Qu, Z., Blumm, N., Barabasi, A.-L.: Limits of predictability in human mobility. *Science (New York, N.Y.)* **327**, 1018–21 (2010). doi:[10.1126/science.1177170](https://doi.org/10.1126/science.1177170)
19. Alessandretti, L., Sapiezynski, P., Lehmann, S., Baronchelli, A.: Evidence for a conserved quantity in human mobility. *Nature Human Behaviour* **2** (2018). doi:[10.1038/s41562-018-0364-x](https://doi.org/10.1038/s41562-018-0364-x)
20. Wang, D., Pedreschi, D., Song, C., Giannotti, F., Barabasi, A.-L.: Human mobility, social ties, and link prediction. *Proceedings of the ACM SIGKDD International Conference on Knowledge Discovery and Data Mining*, 1100–1108 (2011). doi:[10.1145/2020408.2020581](https://doi.org/10.1145/2020408.2020581)
21. Fan, C., Liu, Y., Huang, J., Rong, Z., Zhou, T.: Correlation between social proximity and mobility similarity. *Scientific Reports* **7** (2016). doi:[10.1038/s41598-017-12274-x](https://doi.org/10.1038/s41598-017-12274-x)
22. Yang, D., Qu, B., Yang, J., Cudre-Mauroux, P.: Revisiting user mobility and social relationships in lbsns: A hypergraph embedding approach, pp. 2147–2157 (2019). doi:[10.1145/3308558.3313635](https://doi.org/10.1145/3308558.3313635)
23. Pappalardo, L., Rinzivillo, S., Simini, F.: Human mobility modelling: Exploration and preferential return meet the gravity model. *Procedia Computer Science* **83** (2016). doi:[10.1016/j.procs.2016.04.188](https://doi.org/10.1016/j.procs.2016.04.188)
24. Barbosa, H., de Lima-Neto, F.B., Evsukoff, A., Menezes, R.: The effect of recency to human mobility. *EPJ Data Science* **4**(1), 21 (2015). doi:[10.1140/epjds/s13688-015-0059-8](https://doi.org/10.1140/epjds/s13688-015-0059-8)
25. Jiang, S., Yang, Y., Gupta, S., Veneziano, D., Athavale, S., Gonzalez, M.C.: The timegeo modeling framework for urban mobility without travel surveys. *Proceedings of the National Academy of Sciences* **113**, 201524261 (2016). doi:[10.1073/pnas.1524261113](https://doi.org/10.1073/pnas.1524261113)
26. Pappalardo, L., Barlacchi, G., Simini, F., Pellungrini, R.: scikit-mobility: a python library for the analysis, generation and risk assessment of mobility data (2019)
27. Liu, X., Chen, H., Andris, C.: trajgans : Using generative adversarial networks for geo-privacy protection of trajectory data (vision paper). (2018)

Appendix

GeoSim_d

A modeling limit of GeoSim concerns the spatial patterns of the generated synthetic trajectories. GeoSim does not take into account the distance from the current location and the location to explore [16], since the destination of the next move is chosen uniformly at random. Consequently, the probability density functions for both jump size and radius of gyration of the generated trajectories do not follow the proper empirical distribution [4].

The power-law behavior of the probability density function of the jump length suggests that individuals are more likely to move at small rather than long distances. To take into account this observation in the first extension of GeoSim, namely GeoSim_d, in the Exploration-Individual action an agent a currently at location r_j , selects an unvisited location r_i , with $i \in \text{exp}_a$, with probability $p(r_i) \propto \frac{1}{d_{ij}}$ where d_{ij} is the geographic distance between location r_i and r_j .

GeoSim_{gravity}

Individuals do not consider the distance from a place as the only discriminant factor while selecting the next location to explore. They are driven by a preferential-exploration force in the selection of the new location to explore [23, 2]. The individuals take into account also the relevance of a location at a collective level together

with the distance from their current location. The method used for coupling both the distance and the relevance is the same used in the d -EPR model [23]: the use of a gravity law. The usage of the gravity model is justified by the accuracy of the gravity model to estimate origin-destination matrices even at the country level [23].

In $\text{GeoSim}_{gravity}$, the second proposed extension of GeoSim, an agent a currently at location r_j , during the Exploration-Individual action selects an unvisited location r_i , with $i \in \text{exp}_a$, with probability $p(r_i) \propto \frac{w_i w_j}{d_{ij}^2}$ where d_{ij} is the geographic distance between location r_i and r_j and w_i, w_j represent their relevance.

The relevance of a location can be estimated through the measure visits per location (Sect. 4.1), using a real mobility dataset. In case the real information is not available, the relevance of a location can be estimated using the population density [2].